



THE HONG KONG
POLYTECHNIC UNIVERSITY

香港理工大學

Pao Yue-kong Library

包玉剛圖書館

Copyright Undertaking

This thesis is protected by copyright, with all rights reserved.

By reading and using the thesis, the reader understands and agrees to the following terms:

1. The reader will abide by the rules and legal ordinances governing copyright regarding the use of the thesis.
2. The reader will use the thesis for the purpose of research or private study only and not for distribution or further reproduction or any other purpose.
3. The reader agrees to indemnify and hold the University harmless from and against any loss, damage, cost, liability or expenses arising from copyright infringement or unauthorized usage.

IMPORTANT

If you have reasons to believe that any materials in this thesis are deemed not suitable to be distributed in this form, or a copyright owner having difficulty with the material being included in our database, please contact lbsys@polyu.edu.hk providing details. The Library will look into your claim and consider taking remedial action upon receipt of the written requests.

The Hong Kong Polytechnic University

Department of Applied Physics

Critical Behavior of the Random-bond Clock Model

WU Pak Hong Raymond

A thesis submitted in partial fulfillment of the requirements for
the degree of Master of Philosophy

August 2012

CERTIFICATE OF ORIGINALITY

I hereby declare that this thesis is my own work and that, to the best of my knowledge and belief, it reproduces no material previously published or written, nor material that has been accepted for the award of any other degree or diploma, except where due acknowledgement has been made in the text.

_____ (Signed)

_____ WU Pak Hong Raymond (Name of student)

Abstract

The critical behavior of the clock model in two-dimensional square lattice is studied numerically using Monte Carlo method with Wolff algorithm. The Kosterlitz-Thouless (KT) transition is observed in the six-state clock model, where an intermediate phase exists between the low-temperature ordered phase and the high-temperature disordered phase. The bond randomness is introduced to the system by assuming a Gaussian distribution for the coupling coefficients with the mean $\mu=1$ and different values of variance, from $\sigma^2=0.1$ to $\sigma^2=3.0$. An abrupt jump in the helicity modulus at the transition, which is the key characteristic of the KT transition, is verified with a stability argument. The critical temperature T_c for both pure and disordered systems is determined from the critical exponent $\eta(T_c)=1/4$. The results showed that a small amount of disorder (small σ) reduces the critical temperature of the system, without altering the nature of transition. However, a larger amount of disorder changes the transition from the KT-type into that of non-KT-type.

Publications arising from the thesis

Raymond P. H. Wu, Veng-cheong Lo, and Haitao Huang, “Critical behavior of two-dimensional spin systems under the random-bond six-state clock model,” *Journal of Applied Physics*, vol. 112, p. 063924, 2012.

Raymond P. H. Wu, Veng-cheong Lo, and Haitao Huang, “Critical behavior of the random-bond clock model,” *AIP Conference Proceedings*, vol. 1476, p. 253, 2012.

Acknowledgements

I would like to acknowledge the support of the Department of Applied Physics, The Hong Kong Polytechnic University, in particular my supervisors Dr. LO Veng Cheong and Dr. HUANG Haitao.

Table of contents

Abstract	3
Publications arising from the thesis	4
Acknowledgements	5
Table of contents	6
List of figures	8
List of tables	11
Chapter 1 Introduction	12
1.1 Critical phenomena	12
1.2 Spin models.....	13
1.3 Phase transition	19
1.4 Kosterlitz-Thouless transition	21
1.5 Disordered systems	22
Chapter 2 Theory	24
2.1 Model	24
2.2 Magnetization, specific heat, and susceptibility	25
2.3 Helicity modulus and fourth-order helicity modulus.....	26
2.4 Critical exponent and critical temperature	28
Chapter 3 Monte Carlo Methods.....	30
3.1 Random number generator.....	30
3.2 Gaussian distribution.....	30
3.3 Metropolis algorithm.....	33
3.4 Wolff algorithm	33
3.5 Data structure	35

3.6 Boundary conditions	38
3.7 Initialization	38
3.8 Equilibration.....	38
Chapter 4 Results and discussion.....	44
4.1 Metropolis algorithm and Wolff algorithm	44
4.2 Second-order phase transition and KT transition.....	52
4.3 Six-state clock model and eight-state clock model.....	66
4.4 Random-bond six-state clock model and random-bond eight-state clock model.....	73
Chapter 5 Conclusion.....	84
References	87

List of figures

Figure 3.1 The sequence of spins added to the cluster using the first in/first out buffer.	36
Figure 3.2 The sequence of spins added to the cluster using the last in/first out buffer.	37
Figure 3.3 The energy against Monte Carlo step for the clock model with lattice size $N = 128 \times 128$ at temperature $T = 1.5$	40
Figure 3.4 The magnetization against Monte Carlo step for the clock model with lattice size $N = 128 \times 128$ at temperature $T = 1.5$	41
Figure 4.1 The magnetization against temperature for the four-state clock model with lattice size $N = 128 \times 128$ obtained by the Metropolis algorithm and the Wolff algorithm.	46
Figure 4.2 The specific heat against temperature for the four-state clock model with lattice size $N = 128 \times 128$ obtained by the Metropolis algorithm and the Wolff algorithm.	47
Figure 4.3 The susceptibility against temperature for the four-state clock model with lattice size $N = 128 \times 128$ obtained by the Metropolis algorithm and the Wolff algorithm.	48
Figure 4.4 The magnetization against temperature for the six-state clock model with lattice size $N = 128 \times 128$ obtained by the Metropolis algorithm and the Wolff algorithm.	49
Figure 4.5 The specific heat against temperature for the six-state clock model with lattice size $N = 128 \times 128$ obtained by the Metropolis algorithm and the Wolff algorithm.	50

Figure 4.6 The susceptibility against temperature for the six-state clock model with lattice size $N = 128 \times 128$ obtained by the Metropolis algorithm and the Wolff algorithm.	51
Figure 4.7 The magnetization against temperature for the four-state clock model with various lattice sizes.	55
Figure 4.8 The magnetization against temperature for the six-state clock model with various lattice sizes.	56
Figure 4.9 The specific heat against temperature for the four-state clock model with various lattice sizes.	57
Figure 4.10 The specific heat against temperature for the six-state clock model with various lattice sizes.	58
Figure 4.11 The susceptibility against temperature for the four-state clock model with various lattice sizes.	59
Figure 4.12 The susceptibility against temperature for the six-state clock model with various lattice sizes.	60
Figure 4.13 The helicity modulus against temperature for the four-state clock model with various lattice sizes.	61
Figure 4.14 The helicity modulus against temperature for the six-state clock model with various lattice sizes.	62
Figure 4.15 The fourth-order helicity modulus against temperature for the six-state clock model with various lattice sizes.	63
Figure 4.16 The critical exponent η against temperature for the six-state clock model with various lattice sizes.	64
Figure 4.17 The magnetization against temperature for the eight-state clock model with various lattice sizes.	68
Figure 4.18 The specific heat against temperature for the eight-state clock	

model with various lattice sizes.....	69
Figure 4.19 The susceptibility against temperature for the eight-state clock model with various lattice sizes.	70
Figure 4.20 The helicity modulus against temperature for the eight-state clock model with various lattice sizes.	71
Figure 4.21 The fourth-order helicity modulus against temperature for the eight-state clock model with various lattice sizes.	72
Figure 4.22 The magnetization against temperature for the random-bond six-state clock model with lattice size $N = 128 \times 128$ and various σ^2	76
Figure 4.23 The specific heat against temperature for the random-bond six-state clock model with lattice size $N = 128 \times 128$ and various σ^2	77
Figure 4.24 The susceptibility against temperature for the random-bond six-state clock model with lattice size $N = 128 \times 128$ and various σ^2	78
Figure 4.25 The helicity modulus against temperature for the random-bond six-state clock model with lattice size $N = 128 \times 128$ and various σ^2	79
Figure 4.26 The fourth-order helicity modulus against temperature for the random-bond six-state clock model with lattice size $N = 128 \times 128$ and various σ^2	80
Figure 4.27 The critical exponent η against temperature for the random-bond six-state clock model with lattice size $N = 128 \times 128$ and various σ^2	81
Figure 4.28 The critical temperature against σ^2 for the random-bond six-state clock model with lattice size $N = 128 \times 128$	83

List of tables

Table I The relaxation time for the six-state clock model with various lattice sizes at temperature $T = 1.5$	42
Table II The relaxation time for the random-bond six-state clock model with $\sigma^2 = 3.0$ and various lattice sizes at temperature $T = 1.5$	43
Table III The critical temperature for the six-state clock model with various lattice sizes.	65
Table IV The critical temperature for the random-bond six-state clock model with lattice size $N = 128 \times 128$ and various σ^2	82

Chapter 1 Introduction

1.1 Critical phenomena

Magnetism has long been studied because it is related to many different areas in physics. Maxwell combined electricity and magnetism into electromagnetism in his famous set of equations [1, 2], which describes the electromagnetic properties of a system macroscopically. From special relativity [3], the origin of magnetism is unveiled as the effect of relative motion between electric charges. From quantum mechanics [4], it is found that the spin of an electron results in a magnetic moment with one of a set of discrete values. Magnetic materials are the materials in which some properties change in response to a magnetic field. One important quantity is the magnetization. In any system, the magnetization can be calculated by the sum of all these magnetic moments. However, because of the tremendously large number of atoms in an ordinary matter, it is impractical to handle every magnetic moment, as well as to derive the magnetic properties from them. The problem with such statistical nature can be studied by statistical mechanics with much reduced effort.

In statistical mechanics, ferromagnetic systems can be described by various spin models such as the Ising model [5, 6] and the Potts model [7]. In a ferromagnetic system, non-zero magnetization is developed below a critical temperature T_c . As the temperature increase above T_c , the magnetization becomes zero and the system becomes paramagnetic. If the

system is cooled down again, just below T_c , the ferromagnetic phase recurs again. The transition from paramagnetic phase to ferromagnetic phases is important for both technological applications and academic interests. The study of phase transition is in the area of critical phenomena.

In our daily life, we often encounter various forms of phase transition, such as the transformations of solid, liquid, and gas. The phase transition from water to ice is perceived to be entirely different to that from paramagnetic to ferromagnetic material. Surprisingly, the critical properties of both systems can be described by the same model. At the transition, the details of the physical system are not important and the properties of the system are only governed by the critical exponents. Different models with the same critical exponents are said to belong to the same universality class. It happens that, a single model elaborated to study certain phenomenon is found to be useful in studying another physical situation with the same universality class. This is the universality in the critical phenomena. Another interesting feature in the critical phenomena is the emergence of spontaneous order, such as the spontaneous magnetization in ferromagnetic system. This kind of collective behavior is also manifested in many other systems, such as the traffic systems, the stock markets, and the organization of life. Therefore, the study of critical phenomena is indeed cross-disciplinary and promises important applications in many areas.

1.2 Spin models

To illustrate the above ideas on critical phenomena, several spin

models will be introduced. In statistical mechanics, spin models are developed to describe ferromagnetism. The central idea of spin models is to simplify the problem, so that it is mathematically manageable while retaining the essential physics of the system. The Ising model is the simplest and the most studied spin model among others. Though simple, it provides an example for many important ideas on critical phenomena.

In the Ising model, an ensemble of spins is defined on an array of lattice points. Without loss of generality, a two-dimensional lattice space is used. A spin located at the lattice site i is denoted by the spin state S_i . For simplicity, we assumed the spins interact with their nearest neighbors only. The Hamiltonian of the Ising model is given by

$$H = -\sum_{\langle ij \rangle} J_{ij} S_i S_j - \sum_i h_i S_i, \quad (1.1)$$

where $\langle ij \rangle$ denotes the summation is over the nearest neighbors only. In the Ising model, the spin orientation is restricted to one of the two opposite directions and S_i takes two scalar values, being $+1$ for spin up and -1 for spin down, with referencing to the external field. The strength of interaction between spins S_i and S_j is determined by the coupling coefficient J_{ij} which is usually assumed to be a constant J . The signs are conventional. A positive J value indicates a ferromagnetic system, where the energy is lowered by aligning the spins in the same direction. On the contrary, a negative J value makes the neighboring spins oppositely aligned and results in an antiferromagnetic system. Furthermore, the external field acting on spin S_i is h_i .

The Ising model is not restricted to describe ferromagnetism only. In the Ising model, the two orientations of spin can be viewed as two variants of the other type of physical property, such as a binary system of a mixture of two different kinds of atoms. This demonstrates the generality and wide applicability of the Ising model.

As a model developed to describe ferromagnetism, the Ising model is expected to demonstrate the transition from the paramagnetic phase to the ferromagnetic phase. Analytic solution exists for the one-dimensional and the two-dimensional Ising model, but it remains unknown for the three-dimensional case. Surprisingly, there is no phase transition for the one-dimensional Ising model. In the one-dimensional Ising model, the ordering of spins cannot be developed due to the thermal fluctuations acting on the system. Hence the ferromagnetic phase does not exist, except at the zero temperature. Nevertheless, phase transition does exist for the two-dimensional Ising model.

For the Ising model in the absence of external field, the properties of the system remain unchanged if all the spin values are switched. Then the system is known to have the Z_2 symmetry. At the transition, spontaneous order is developed, which brings the system from a symmetrical state into one of the two definite, asymmetrical states. The Z_2 symmetry is broken and infinitesimal small fluctuations will decide the fate of the system by determining which branch of bifurcation is taken. This phenomenon is described as spontaneous symmetry breaking.

At the neighborhood of the critical point, the properties of the system have power-law relationship associating with the specific heat C , the magnetization M , and the susceptibility χ :

$$C \propto t^{-\alpha}, \quad (1.2)$$

$$M \propto t^\beta, \quad (1.3)$$

$$\chi \propto t^{-\gamma}, \quad (1.4)$$

where $t \equiv (T - T_c)/T_c$ is the reduced temperature. Furthermore, the external field H is related by

$$H \propto M^\delta, \quad (1.5)$$

where α , β , γ , and δ are the critical exponents. At the transition, the details of the physical system are not important and the properties of the system are only governed by the critical exponents. The exact values of the critical exponents for the Ising model obtained from mean-field theory are

$$\alpha = 0, \quad (1.6)$$

$$\beta = \frac{1}{2}, \quad (1.7)$$

$$\gamma = 1, \quad (1.8)$$

$$\delta = 3. \quad (1.9)$$

It is worth mentioning that in a van der Waals system governed by the equation

$$\left(p + \frac{a}{v^2}\right)(v - b) = kT, \quad (1.10)$$

a liquid-gas phase transition occurs at the critical temperature T_c . Near the critical point, the properties of the system have the following power-law relationships associating with the isochoric specific heat C_v , the density difference between the liquid and the gas phase $\rho_l - \rho_g$, the isothermal compressibility κ_T , and the pressure near the critical point $P - P_c$:

$$C_v \propto t^{-\alpha}, \quad (1.11)$$

$$\rho_l - \rho_g \propto (T_c - T)^\beta, \quad (1.12)$$

$$\kappa_T \propto (T - T_c)^{-\gamma}, \quad (1.13)$$

$$P - P_c \propto (\rho - \rho_c)^\delta, \quad (1.14)$$

where the exact values of the critical exponents are

$$\alpha = 0, \quad (1.15)$$

$$\beta = \frac{1}{2}, \quad (1.16)$$

$$\gamma = 1, \quad (1.17)$$

$$\delta = 3. \quad (1.18)$$

These are similar to those in the Ising model with a change of variables $\rho_l - \rho_g$ to M , κ_T to χ , and $P - P_c$ to H . In the van der Waals system, the physical situation is entirely different from that in the Ising model. The former describes the liquid-gas phase transition and the latter describes the paramagnetic-ferromagnetic phase transition. Surprisingly, the critical exponents for both systems are essentially the same and they belong to the same universality class. This shows the fascinating universality of the critical phenomena.

The Ising model can be generalized to other more sophisticated models to tackle different physical situations. The Potts model is one of the generalizations of the Ising model. In the q -state Potts model, the spins can take q different states rather than only two in the Ising model. The Hamiltonian of the Potts model is given by

$$H = -\sum_{\langle ij \rangle} J_{ij} \delta(S_i, S_j) - \sum_i h_i S_i, \quad (1.19)$$

where $\delta(S_i, S_j)$ is the Kronecker delta which equals to 1 if $S_i = S_j$ and 0 otherwise. The spins can be viewed as unit vectors pointing in the q symmetrical directions of a hypertetrahedron in $q-1$ dimensions and the state of a spin is denoted by a value from 0 to $q-1$. In Potts model, only the spins with the same state are interacting, as manifested by the Kronecker delta. The Potts model is significantly important for both physical and mathematical study. For example, the antiferromagnetic Potts model is related to the famous coloring problem in mathematics. Apart from the Potts model, another generalization of the Ising model is the XY model. In the XY model, the spins are confined in a plane and they can orientate in any arbitrary direction from $-\pi$ to π . Hence, the state of a spin varies continuously. The Hamiltonian of the XY model is given by

$$H = -\sum_{\langle ij \rangle} J_{ij} \cos(\theta_i - \theta_j) - \sum_i h_i \cos \theta_i. \quad (1.20)$$

Another generalization of the Ising model is the clock model, which is a discrete version of the XY model. In the q -state clock model, the spins are confined in a plane with q different orientations, each of which is specified by a phase angle

$$\theta_n = n \left(\frac{2\pi}{q} \right), \quad (1.21)$$

where $n = 0, 1, 2, \dots, q-1$ denotes the state of a spin. The Hamiltonian of the clock model is given by

$$H = -\sum_{\langle ij \rangle} J_{ij} \cos(\theta_i - \theta_j) - \sum_i h_i \cos \theta_i. \quad (1.22)$$

There are also other spin models such as the Heisenberg model and the more general $O(n)$ model, but they are beyond our scope.

1.3 Phase transition

From the classification suggested by Ehrenfest, the phase transition can be classified by the lowest order of derivatives of the free energy of the system that shows discontinuity with respect to some thermodynamic variables. To be more precise, the magnetization is the first order derivative of the free energy with respect to the external field. The specific heat and the susceptibility are the second order derivatives with respect to the temperature and the external field, respectively. Hence, in a first-order phase transition, the magnetization is discontinuous, while in a second-order phase transition the magnetization is continuous, but the specific heat and the susceptibility are discontinuous. Furthermore, in the first-order phase transition, a fixed amount of energy, called the latent heat, is absorbed or released. However, in the second-order phase transition, no latent heat is involved. A familiar example of the first-order phase transition is the phase transition from water to ice, in which the latent heat can be measured easily.

Apart from the above classification, Landau developed a phenomenology theory for the phase transition based on the symmetry in the Hamiltonian of the system [8]. The free energy of the system $F(m, T)$ is expressed as a power series of order parameter m given by

$$F(m, T) = -hm + a(T) + b(T)m^2 + c(T)m^4 + \dots \quad (1.23)$$

The symmetry in the Hamiltonian is reflected by the free energy that

$$F(-m, T) = F(m, T). \quad (1.24)$$

This gives an insight on the symmetry breaking phenomenon at the phase transition and it is very useful in calculating the critical exponents of the

system. Although it is a type of mean-field theory, which does not account for the fluctuations in the system, it gives inspiration which leads to the more general theory, the Ginzburg-Landau theory [9].

Most phase transitions, including those exhibited by the Ising model and the Potts model belong to either the first-order type or the second-order type. The transition from paramagnetic phase to ferromagnetic phase is determined by the competition between the spin-spin interactions and the thermal fluctuations acting on the system. In these systems, spontaneous symmetry breaking occurred and long-range order is developed at the transition. The phase transition is determined by the free energy of the system, which is given by

$$F = E - TS . \quad (1.25)$$

The interactions of spins tend to introduce order to the system, which decrease the energy and the entropy. On the other hand, the thermal fluctuations tend to destroy the order of the system, which increase the energy and the entropy. The critical temperature is determined by minimizing the free energy of the system. In the high-temperature disordered phase, the interactions of spins tend to break the symmetry and transforms to the order phase, while the thermal fluctuations acting on the system tend to restore the symmetry.

In the Ising model, the system undergoes a second-order phase transition. In the Potts model, the phase transition is of the second-order for $q \leq 4$, and of the first-order for $q > 4$. However, the phase transition in the two-dimensional XY model is neither first-order nor second-order. The

system undergoes a specific phase transition called the Kosterlitz-Thouless (KT) transition, which is of the infinite-order.

1.4 Kosterlitz-Thouless transition

Apart from the ordinary first-order and the second-order phase transitions manifested in most spin models, a specific phase transition called the Kosterlitz-Thouless (KT) transition is observed in superfluid systems and it can be described by the two-dimensional XY model [10-12]. Unlike the first-order and second-order phase transitions, the KT transition in the two-dimensional system with continuous symmetry does not involve symmetry breaking. Furthermore, the long-range order of the system in the low-temperature phase cannot be developed because of the existence of spin waves. The driving force behind the KT transition involves the topological excitation of vortices, which plays the role of charges in the system. The excitation of vortices requires energy and gives additional entropy to the system. Furthermore, the topological charges have long-range interactions in the system and we called that as quasi-long-range order. The mechanism of the KT transition is entirely different from the simple spin-spin interaction in other spin models and it gives a good example of the interesting emergent phenomena in the system.

The q -state clock model is a discrete version of the XY model. For $q = 2$, the clock model reduces to the Ising model, while for $q = 3$, it is equivalent to the three-state Potts model, and for $q = 4$, it is also called the Ashkin-Teller model [13], which is the four-component version of the Ising

model. At the limiting case $q \rightarrow \infty$, where the spin state varies continuously, it is restored to the XY model. It is known that, the phase transition in the Ising model is of the second-order type, while that in the XY model is of the KT-type. The clock model, being a bridge between different models, is expected to have various critical behavior under different values of q . Extensive studies [14-21] on the clock model had shown that, for $q \leq 4$, the phase transition is Ising-like, and for $q > 6$, it is XY -like. There is still no conclusive result for the case where $q = 5$ [15, 21-23]. Since the critical behavior for the q -state clock model does not change appreciably on varying q values when q is large. This means that, without using the XY model, which involves the continuous spin states, the six-state clock model ($q = 6$) can be used to study the KT transition.

1.5 Disordered systems

The presence of defects interrupts the periodic structure of crystalline materials and the systems become disordered when the quantity of interruptions is large. It can be visualized by a random distribution of coupling coefficients between neighboring spins. The effects of disorder on phase transition have attracted many interests [24-26]. In some systems, a small amount of disorder can have dramatic effects and even changes the nature of phase transition [25]. A number of numerical works [27-29] had studied the effects of non-magnetic impurities on the KT transition. Since non-magnetic impurities can be viewed as lattice vacancies, the results found that the KT transition disappears as the vacancy density reaches the lattice percolation limit. In real systems, the source of defects may not be

only from the non-magnetic impurities but can also from the magnetic ones. In statistical point of view, it is natural to consider a Gaussian distribution for the coupling coefficients. Theoretical works [30] conjectured that strong disorder will induce a first-order phase transition in the XY model. It is our motivation to study the effects of disorder on the phase transition in the six-state clock model.

Chapter 2 Theory

2.1 Model

We consider an ensemble of spins on a two-dimensional square lattice with size $N = L \times L$. For simplicity, we assumed the spins interact with their nearest neighbors only. In the q -state clock model, the spins are confined in a plane with q different orientations each of which is specified by a phase angle

$$\theta_n = n \left(\frac{2\pi}{q} \right), \quad (2.1)$$

where $n = 0, 1, 2, \dots, q-1$ denotes the state of a spin. The Hamiltonian of the clock model takes the form $H = -\sum_{\langle ij \rangle} K(\theta_{ij})$, where $\langle ij \rangle$ denotes the summation is over the nearest neighbors only and $\theta_{ij} = \theta_j - \theta_i$ is the phase angle difference between two spins at lattice sites i and j . The function $K(\theta)$ is periodic with a period 2π . One simple form for $K(\theta)$ is $K(\theta) = J \cos \theta$, where J is the coupling coefficient between two neighboring spins. The Hamiltonian is then given by

$$H = -\sum_{\langle ij \rangle} J_{ij} \cos(\theta_i - \theta_j). \quad (2.2)$$

The spin at spin state n can also be denoted by the spin vector

$$\mathbf{S}_n = (\sin \theta_n, \cos \theta_n). \quad (2.3)$$

Subsequently, the Hamiltonian can be expressed as

$$H = -\sum_{\langle ij \rangle} J_{ij} \mathbf{S}_i \cdot \mathbf{S}_j. \quad (2.4)$$

Usually, the coupling coefficients J_{ij} are assumed to be a constant J . A

positive J value indicates a ferromagnetic system, where the energy is lowered by aligning the spins in the same direction. On the contrary, a negative J value makes the neighboring spins oppositely aligned and results in an antiferromagnetic system. To investigate the effect of disorder, the coupling coefficients J_{ij} are assumed to follow the Gaussian distribution

$$P(J) = \frac{1}{\sqrt{2\pi\sigma^2}} \exp\left[-\frac{(J-\mu)^2}{2\sigma^2}\right], \quad (2.5)$$

where $\mu=1$ is the mean and σ^2 is the variance of the distribution. The bond randomness is reflected by the parameter σ . In particular, $\sigma^2=0$ represents a pure system with no disorder and with constant coupling coefficient $J=1$.

2.2 Magnetization, specific heat, and susceptibility

Several properties of the system are calculated in order to study the phase transitions in the clock model. The energy per spin E of the system is given by

$$E = -\frac{1}{N} \left\langle \sum_{\langle ij \rangle} J_{ij} \mathbf{S}_i \cdot \mathbf{S}_j \right\rangle, \quad (2.6)$$

where $\langle \dots \rangle$ denotes the ensemble average of the quantities. The magnetization per spin \mathbf{m} is given by

$$\mathbf{m} = \left(\left\langle \frac{1}{N} \sum_i \sin \theta_i \right\rangle, \left\langle \frac{1}{N} \sum_i \cos \theta_i \right\rangle \right), \quad (2.7)$$

and its magnitude is represented by m . Furthermore, the specific heat per

spin c can be obtained from the fluctuations of energy and is given by

$$c = \frac{1}{T^2} (\langle E^2 \rangle - \langle E \rangle^2). \quad (2.8)$$

Similarly, the susceptibility per spin χ is given by

$$\chi = \frac{N}{T} (\langle m^2 \rangle - \langle m \rangle^2). \quad (2.9)$$

Throughout the thesis, the temperature T is given as a dimensionless quantity, which is scaled by J/k , where J is the coupling coefficient and k is the Boltzmann constant.

2.3 Helicity modulus and fourth-order helicity modulus

Besides judging the existence of the KT transition from the above properties of the system, the more convincing evidence is by observing the critical behavior of the helicity modulus. Consider the Hamiltonian of the clock model including an externally imposed spin twist $\mathbf{\Delta} = (\Delta_x, \Delta_y)$ across the system

$$H = - \sum_{\langle ij \rangle} J_{ij} \cos(\theta_i - \theta_j - \frac{1}{L} \mathbf{r}_{ij} \cdot \mathbf{\Delta}), \quad (2.10)$$

where \mathbf{r}_{ij} is a unit vector pointing from lattice site i to j . The

components of the spin twist Δ_x and Δ_y are defined by the summation of the phase angle difference θ_{ij} along the \mathbf{x} and \mathbf{y} directions, respectively.

The helicity modulus per spin Υ is a measure of the resistance to an infinitesimal spin twist across the system along one direction. It is related to the free energy per spin F of the system by $\Upsilon \equiv \partial^2 F / \partial \Delta^2 \big|_{\Delta=0}$, which leads to the expression

$$\Upsilon = -\frac{1}{2}\langle E \rangle - \frac{N}{T}\langle s^2 \rangle, \quad (2.11)$$

where

$$s \equiv \frac{1}{N} \sum_{\langle ij \rangle} J_{ij} \sin(\theta_i - \theta_j) (\mathbf{r}_{ij} \cdot \mathbf{x}). \quad (2.12)$$

According to the renormalization group calculations [11], the helicity modulus in the XY model which undergoes the KT transition jumps from the value $(2/\pi)T_c$ to zero at the transition in the thermodynamic limit. This abrupt jump in the helicity modulus at the transition is the key feature of the KT transition. Unfortunately, it is very difficult to determine the discontinuity of the helicity modulus from numerical calculations because of the limited precision.

A new numerical method [31] based on a stability argument can be used to identify the KT transition. The expansion of free energy of the system gives $F(\Delta) = \langle \Upsilon \rangle \frac{\Delta^2}{2!} + \langle \Upsilon_4 \rangle \frac{\Delta^4}{4!} + \dots$, where $\Upsilon_4 \equiv \partial^4 F / \partial \Delta^4 \big|_{\Delta=0}$ is the fourth-order helicity modulus and it can be expressed as

$$\langle \Upsilon_4 \rangle = \frac{1}{2N} \langle E \rangle + \frac{3}{4T} \langle E^2 \rangle - \frac{3}{4T} \langle E^2 \rangle + \frac{4}{T} \langle s^2 \rangle + \frac{3N^2}{T^3} \langle s^2 \rangle^2 + \frac{3N}{T^2} \langle E \rangle \langle s^2 \rangle. \quad (2.13)$$

A spin twist to the system gives an additional contribution to the free energy so that $F(\Delta) \geq F(0)$. Since the helicity modulus Υ must be non-negative and in the XY model, this quantity is positive and finite below the critical temperature and is zero above it. Consequently, the fourth-order helicity modulus Υ_4 must also be non-negative at any temperature where Υ vanishes. Supposed Υ_4 is negative at the transition, then Υ cannot approach zero continuously but must make a discontinuous jump to zero at the transition instead. Hence we can distinguish the KT transition from the

ordinary first-order or the second-order phase transition by the fourth-order helicity modulus.

2.4 Critical exponent and critical temperature

From the theory developed by Kosterlitz [11], it is known that at $T \rightarrow T_c$, the correlation length ξ and the susceptibility χ in the XY model diverge according to the asymptotic laws

$$\xi \propto \exp(bt^{-\frac{1}{2}}), \quad (2.14)$$

where $t \equiv (T - T_c)/T_c$ and $b \approx 1.5$, and

$$\chi \propto \xi^{2-\eta}, \quad (2.15)$$

where the critical exponent $\eta = 1/4$ has the same value as that of the two-dimensional Ising model and is the only exponent in the absence of external field for the XY model. From the studies of the superfluid systems, the helicity modulus is given by $\Upsilon = (\hbar/m)^2 \rho_s$, where m is the mass of the superfluid and ρ_s is density of the superfluid. The critical exponent is given by $\eta = (m^2/2\pi\hbar^2 \rho_s)T$. Then we can obtain a relation

$$\eta = \frac{T}{2\pi\Upsilon}. \quad (2.16)$$

Hence the critical exponent η can be calculated from the helicity modulus Υ . This, in turn, enables us to determine the critical temperature T_c from the point where the critical exponent $\eta(T_c) = 1/4$. Furthermore, since the helicity modulus Υ jumps from the value $(2/\pi)T_c$ to zero at the transition, we can also determine the critical temperature T_c from the intersection of the curve and the straight line

$$\Upsilon = \frac{2}{\pi} T. \quad (2.17)$$

Chapter 3 Monte Carlo Methods

3.1 Random number generator

Previous works [32] had shown that the Wolff algorithm can yield incorrect answers with some “high quality” random number generators. Although the Wolff algorithm can dramatically reduce the critical slowing down, it is very sensitive to the subtle correlations in the random number generators. Therefore, to choose a reliable random number generator for the Wolff algorithm is important.

Comparing the performance of different random number generators for the Wolff algorithm, the 32-bit linear congruential generator with parameters

$$X_n = (16087 X_{n-1}) \bmod (2^{31} - 1), \quad (3.1)$$

is used throughout this work. It generates uniform random numbers $0 \leq r < 1$ and it should be seeded with a non-zero long integer. The value of the seed is also outputted for the checking of the results.

3.2 Gaussian distribution

Transformation method can be used to produce non-uniformly distributed random numbers from uniformly distributed ones. To produce random numbers x distributed according to some function $f(x)$, provided $x_{\min} \leq x < x_{\max}$. The fraction $F(x)$ of these random numbers

which lie below some value x is given by

$$F(x) = \int_{x_{\min}}^x f(x') dx'. \quad (3.2)$$

The same fraction of the uniformly distributed random numbers lies in the interval $0 \leq r < F(x)$. To map numbers from random number generator which falls into this region onto the numbers between x_{\min} and x in the new distribution, the number x in the non-uniform distribution should be generated when the number

$$r = F(x), \quad (3.3)$$

is produced by the uniform generator.

The Gaussian distribution function with mean and variances equal to zero and one, respectively is given by

$$f(x) = \frac{1}{\sqrt{2\pi}} \exp\left(-\frac{x^2}{2}\right). \quad (3.4)$$

The cumulative distribution function is the error function,

$$F(x) = \frac{1}{2} \left[1 + \operatorname{erf}\left(\frac{x}{\sqrt{2}}\right) \right]. \quad (3.5)$$

Unfortunately, there is no known closed-form expression for the error function, which makes it impossible to invert this equation.

The Box-Muller method is used to tackle the problem. It is a two-dimensional variation of the transformation method. Consider the probability,

$$f(x, y) dx dy = \frac{1}{2\pi} \exp\left(-\frac{x^2 + y^2}{2}\right) dx dy, \quad (3.6)$$

in polar coordinates,

$$f(r, \theta) dr d\theta = \frac{1}{2\pi} \exp\left(-\frac{r^2}{2}\right) r dr d\theta. \quad (3.7)$$

The θ variable is a uniformly distributed number where

$$0 \leq \theta < 2\pi. \quad (3.8)$$

The distribution function for r is

$$f(r) = r \exp\left(-\frac{r^2}{2}\right). \quad (3.9)$$

By the transformation method, a number R produced by the uniform random number generator is

$$R = 1 - \exp\left(-\frac{r^2}{2}\right). \quad (3.10)$$

Rearranging for r ,

$$r = \sqrt{-2 \ln(1-R)} \quad (3.11)$$

With this value for r and the random value for θ , the two numbers

$$x = r \sin \theta, \quad (3.12)$$

$$y = r \cos \theta, \quad (3.13)$$

are independent Gaussianly distributed random numbers.

For the Gaussian distribution function $N(\mu, \sigma^2)$ with arbitrary mean and variance,

$$N(\mu, \sigma^2) = \sigma N(0,1) + \mu. \quad (3.14)$$

Then, random numbers following Gaussian distribution with specified mean and variance can be generated.

3.3 Metropolis algorithm

The Metropolis algorithm [33] is the most widely used Monte Carlo algorithm in statistical mechanics, which is a single-spin updating algorithm. In the Metropolis algorithm, a Monte Carlo step (MCS) is described as follows:

- (1) A lattice site i is chosen randomly.
- (2) Consider the spin at lattice site i being updated to a new state, the change of Hamiltonian ΔH is calculated.
- (3) If $\Delta H < 0$, the spin is updated, else update it according to the probability

$$P = \exp\left(-\frac{\Delta H}{T}\right). \quad (3.15)$$

The Metropolis algorithm suffers from a problem called critical slowing down. The correlation time diverges at the transition, which means an infinite sampling time is needed to obtain an accuracy result.

3.4 Wolff algorithm

The Wolff algorithm [34], which is the improvement of the Swendsen-Wang algorithm [35], is applicable to many spin models including the clock model. Instead of updating a single spin, a cluster of spins is updated in the Wolff algorithm to overcome the problem of critical slowing down. We adopted the original idea of Wolff which applies to the XY model. The specialized algorithm for the q -state clock model is described as follows:

- (1) A mirror line is chosen randomly with a normal vector \mathbf{r} .
- (2) A lattice site i is chosen randomly for a cluster formation.
- (3) Spins at the neighboring sites j are added to the cluster according to the probability

$$P = 1 - \exp\left[-\frac{2J_{ij}}{T}(\mathbf{r} \cdot \mathbf{S}_i)(\mathbf{r} \cdot \mathbf{S}_j)\right]. \quad (3.16)$$

- (4) The cluster is updated by reflecting all the spins in the line perpendicular to the normal vector \mathbf{r} .

To implement these procedures, consider the normal vector

$$\mathbf{r}_k = (\sin \phi_k, \cos \phi_k), \quad (3.17)$$

where the angles ϕ_k specifies the state of the normal vector and for even q

$$\phi_k = k \left(\frac{\pi}{q} \right), \quad (3.18)$$

while for odd q

$$\phi_k = \left(k + \frac{1}{2} \right) \left(\frac{\pi}{q} \right), \quad (3.19)$$

where $k = 0, 1, 2, \dots, 2q-1$. Then the phase angle of the reflected spin is given by

$$\mathbf{R}\theta = 2\phi - \theta + \pi, \quad (3.20)$$

where \mathbf{R} is the reflection operator. Then all the combinations for different spin vectors \mathbf{S}_n and normal vectors \mathbf{r}_k can be pre-calculated to reduce the computational cost.

3.5 Data structure

A buffer is a data structure used to store the values of variables temporarily, and retrieve them later. In carrying out the addition of spins to the cluster in the Wolff algorithm, a buffer has to be used to store the spins added to the cluster for the further growth of it. Two types of buffers can be used. They are the first in/first out buffer and the last in/first out buffer. Both buffers are equally efficient, but different cluster growth pattern will be obtained with different buffer being used.

The sequences of spins being added to the cluster using the first in/first out buffer and the last in/first out buffer are given in Figures 3.1 and 3.2, respectively. With the first in/first out buffer, the cluster grows in a spiral fashion, remaining, on average, roughly isotropic throughout its growth. With the last in/first out buffer, the cluster first grows along a line in one direction, and then backs up along its tracks and begins to grow sideways. The Wolff algorithm with the first in/first out buffer is more realistic, especially when the maximum size of a cluster is constrained. Hence, the first in/first out buffer is used throughout this work.

60	53	42	37	50	59	63	64
52	41	30	24	36	49	58	62
39	28	18	13	22	35	48	57
26	16	8	5	11	21	34	47
14	6	2	1	3	9	46	56
25	15	7	4	10	20	33	45
38	27	17	12	19	32	44	55
51	40	29	23	31	43	54	61

Figure 3.1 The sequence of spins added to the cluster using the first in/first out buffer.

57	58	59	60	61	62	63	64
56	55	54	53	52	51	50	49
38	39	40	41	42	43	44	45
37	36	35	34	33	48	47	46
4	3	2	1	32	31	30	29
5	6	7	8	9	10	11	12
20	19	18	17	16	15	14	13
21	22	23	24	25	26	27	28

Figure 3.2 The sequence of spins added to the cluster using the last in/first out buffer.

3.6 Boundary conditions

Since the calculations are carried out on finite size lattice, periodic boundary conditions are applied. The spins at the edge of the lattice are made to interact with the spins at the opposite edge of the lattice. This ensures that all the spins have the same number of neighbors and local geometry. The lattice is completely translational invariant and it can be visualized by considering the two-dimensional lattice being folded into a three-dimensional torus with spins being on the surface of this topological structure.

3.7 Initialization

There are two common choices for the initialization of spins. They are the ground state and the random state. In the first case, all the spins are in the same state. In the random state, the states of the spins are randomly chosen. For the q -state clock model in the absence of external field, there are q different ground states. Since the choice is arbitrary, one of the ground states is chosen as the initial state. However, if the system is in an external field, the ground state will be the state where all the spins are in the direction along the external field. It should be noted that, since Monte Carlo algorithms satisfy the condition of ergodicity, no matter what initial state is chosen, the system will eventually relax to the equilibrium state.

3.8 Equilibration

The system should be in equilibrium before calculating any property of

it. Otherwise, incorrect results will be obtained. The relaxation time defined in terms of Monte Carlo step is the time required for the system to reach equilibrium. Since the properties of the system are in steady state at equilibrium, the simplest way to judge the relaxation time is by observing the properties change over Monte Carlo step. The relaxation time required for the system at the equilibrium state of temperature T_1 to the equilibrium state of temperature T_2 is short if $T_1 \approx T_2$ and it will be long if $T_2 \gg T_1$. Since the ground state ($T = 0$) is chosen as the initial state of the system, we can safely over-estimate the relaxation time by determining it from the system with the highest temperature that we are going to study ($T = 1.5$). The energy and the magnetization against Monte Carlo step for the six-state clock model with lattice size $N = 128 \times 128$ at temperature $T = 1.5$ are given in Figures 3.3 and 3.4, respectively. From the results, it is observed that after approximately 20000 Monte Carlo steps, both the energy and the magnetization become steady and thus it is the relaxation time for the system. Furthermore, longer relaxation time is needed for the disordered system with larger σ^2 . Hence, we can safely over-estimate the relaxation time by determining it from the system with the largest σ^2 that we are going to study ($\sigma^2 = 3.0$). The relaxation time for the six-state clock model with various lattice sizes at temperature $T = 1.5$ is given in Table I. Furthermore, the relaxation time for the random-bond six-state clock model with $\sigma^2 = 3.0$ and various lattice sizes at temperature $T = 1.5$ is given in Table II. It should be noted that, the effect of different values of q and different values of σ^2 on the relaxation time is small.

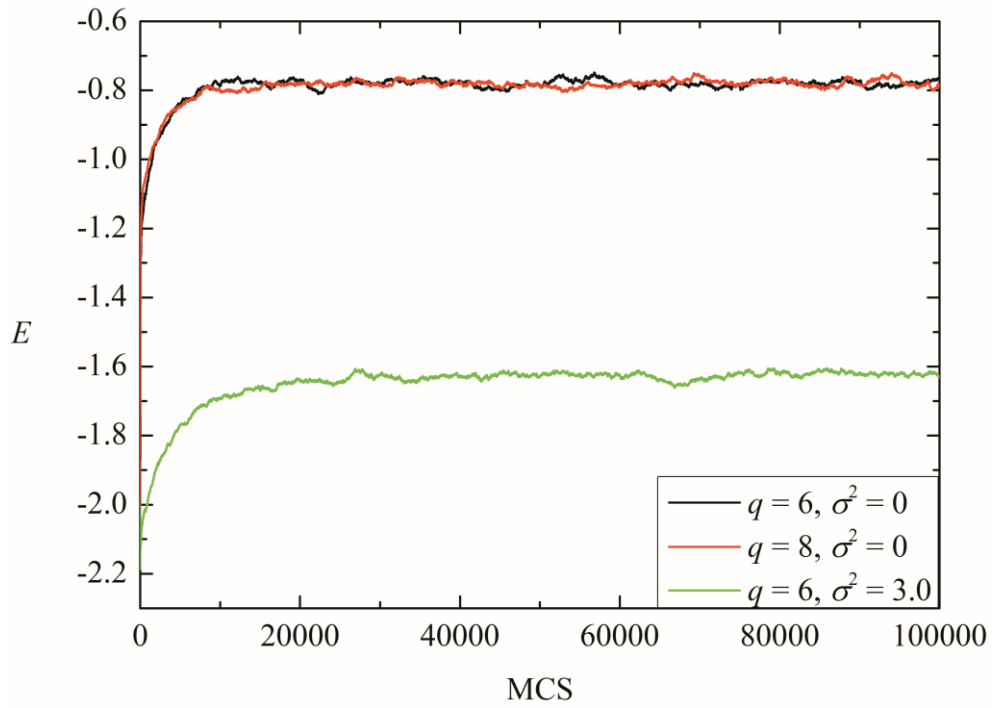


Figure 3.3 The energy against Monte Carlo step for the clock model with lattice size $N = 128 \times 128$ at temperature $T = 1.5$.

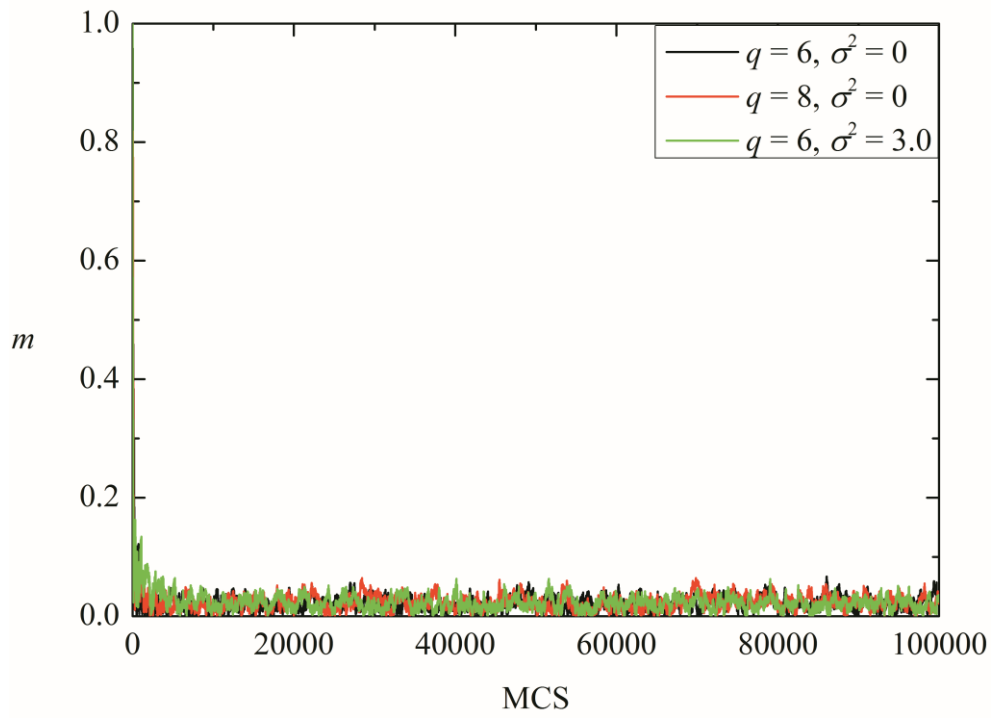


Figure 3.4 The magnetization against Monte Carlo step for the clock model with lattice size $N = 128 \times 128$ at temperature $T = 1.5$.

N	MCS
8×8	2000
16×16	3000
32×32	5000
64×64	10000
128×128	20000

Table I The relaxation time for the six-state clock model with various lattice sizes at temperature $T = 1.5$.

N	MCS
8×8	3000
16×16	5000
32×32	10000
64×64	20000
128×128	40000

Table II The relaxation time for the random-bond six-state clock model with $\sigma^2 = 3.0$ and various lattice sizes at temperature $T = 1.5$.

Chapter 4 Results and discussion

4.1 Metropolis algorithm and Wolff algorithm

The results for the four-state ($q=4$) and the six-state ($q=6$) clock model obtained by the Metropolis algorithm and the Wolff algorithm are shown to demonstrate the difference between these two algorithms.

The magnetization against temperature for the four-state clock model with lattice size $N=128\times 128$ obtained by the Metropolis algorithm and the Wolff algorithm is given in Figure 4.1. The systems undergo phase transition at approximately the same temperature. The results obtained by the Metropolis algorithm give a broader transition than those obtained by the Wolff algorithm. Hence, it is more difficult to determine the critical temperature of the system.

The specific heat and the susceptibility against temperature for the four-state clock model with lattice size $N=128\times 128$ obtained by the Metropolis algorithm and Wolff algorithm are given in Figures 4.2 and 4.3, respectively. The results obtained by the Metropolis algorithm are much noisier than those obtained by the Wolff algorithm. Furthermore, the results obtained by the Metropolis algorithm give a broader peak in both the specific heat and the susceptibility than those obtained by the Wolff algorithm.

The magnetization against temperature for the six-state clock model with lattice size $N = 128 \times 128$ obtained by the Metropolis algorithm and the Wolff algorithm is given in Figure 4.4. The results obtained by both the Metropolis algorithm and the Wolff algorithm undergo two transitions instead of a single one. Again, the results obtained by the Metropolis algorithm give a broader transition than those obtained by the Wolff algorithm. Hence, the intermediate phase for the results obtained by the Metropolis algorithm is not as obvious as that obtained by the Wolff algorithm.

The specific heat and the susceptibility for the six-state clock model with lattice size $N = 128 \times 128$ obtained by the Metropolis algorithm and the Wolff algorithm are given in Figures 4.5 and 4.6, respectively. The results obtained by both the Metropolis algorithm and the Wolff algorithm show a double-peak feature in the specific heat and the susceptibility. However, the results obtained by the Metropolis algorithm are much noisier than those obtained by the Wolff algorithm.

The discrepancy of the results obtained by these algorithms is attributed to the problem of critical slowing down in the Metropolis algorithm, while it does not exist in the Wolff algorithm. However, despite the quantitative difference in the critical temperature, there is no qualitative difference between the results obtained by both algorithms. It is noted that, the computational costs of the Metropolis algorithm and the Wolff algorithm are approximately the same. However, the Wolff algorithm gives much better results. Hence, the Wolff algorithm is used throughout this work.

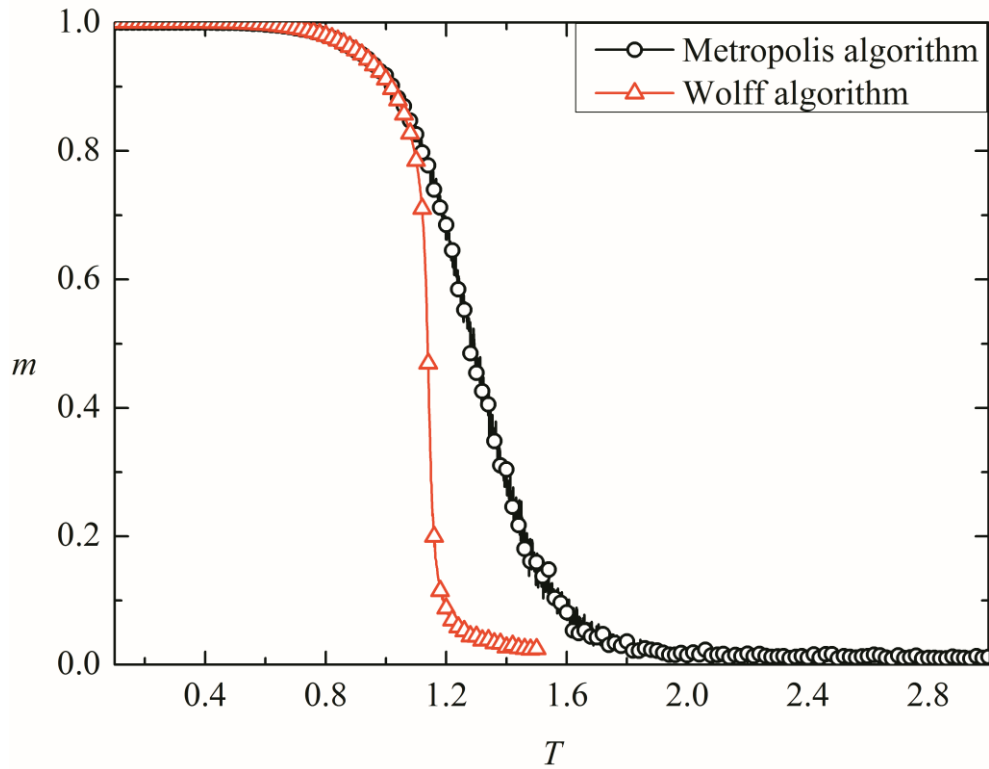


Figure 4.1 The magnetization against temperature for the four-state clock model with lattice size $N=128\times 128$ obtained by the Metropolis algorithm and the Wolff algorithm.

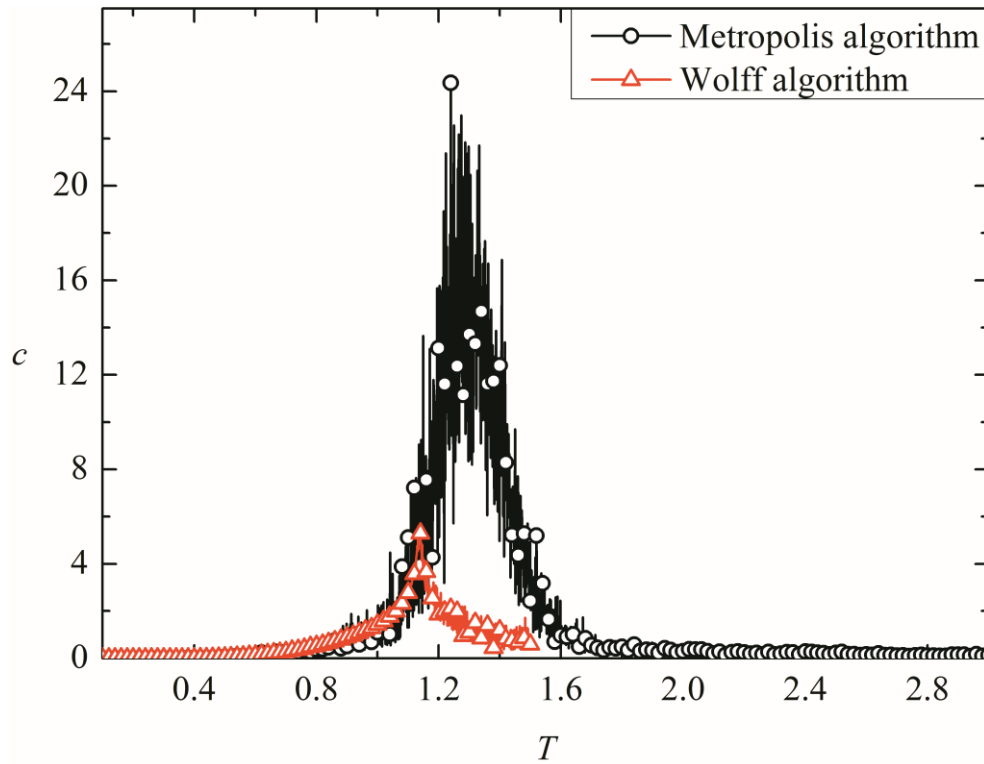


Figure 4.2 The specific heat against temperature for the four-state clock model with lattice size $N=128 \times 128$ obtained by the Metropolis algorithm and the Wolff algorithm.

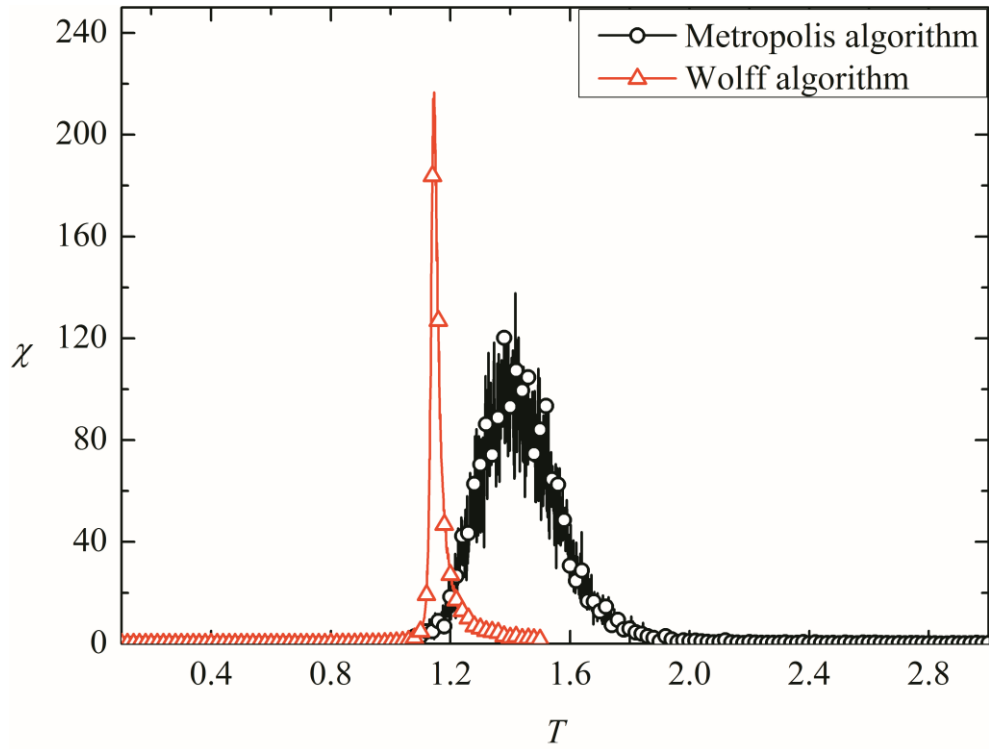


Figure 4.3 The susceptibility against temperature for the four-state clock model with lattice size $N=128 \times 128$ obtained by the Metropolis algorithm and the Wolff algorithm.

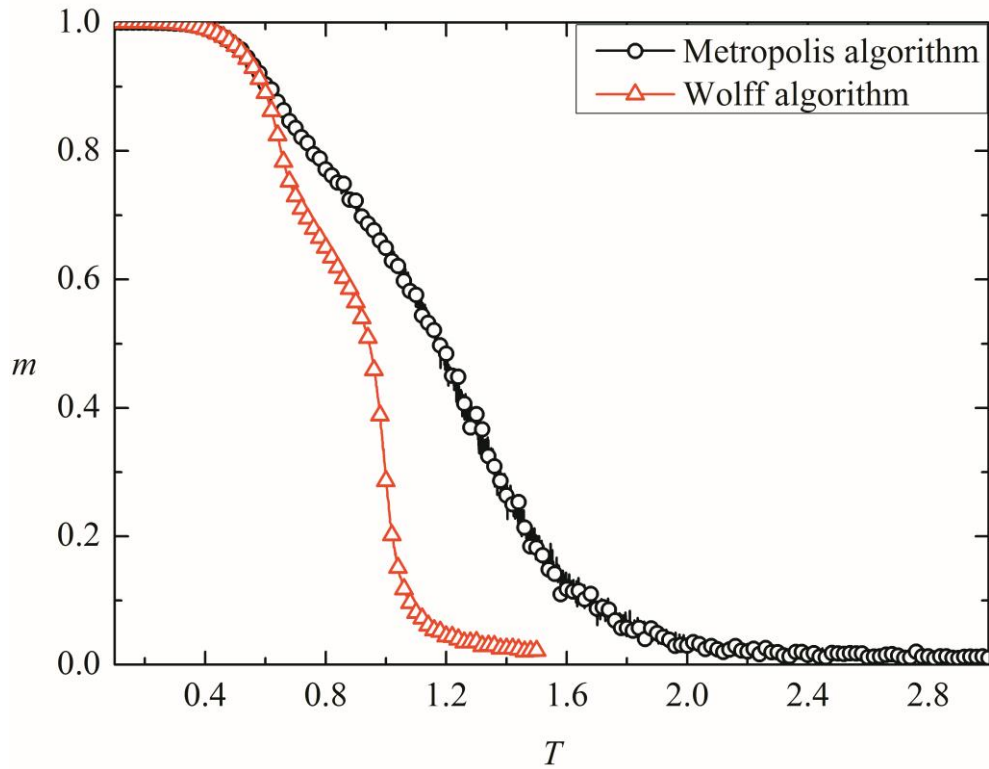


Figure 4.4 The magnetization against temperature for the six-state clock model with lattice size $N = 128 \times 128$ obtained by the Metropolis algorithm and the Wolff algorithm.

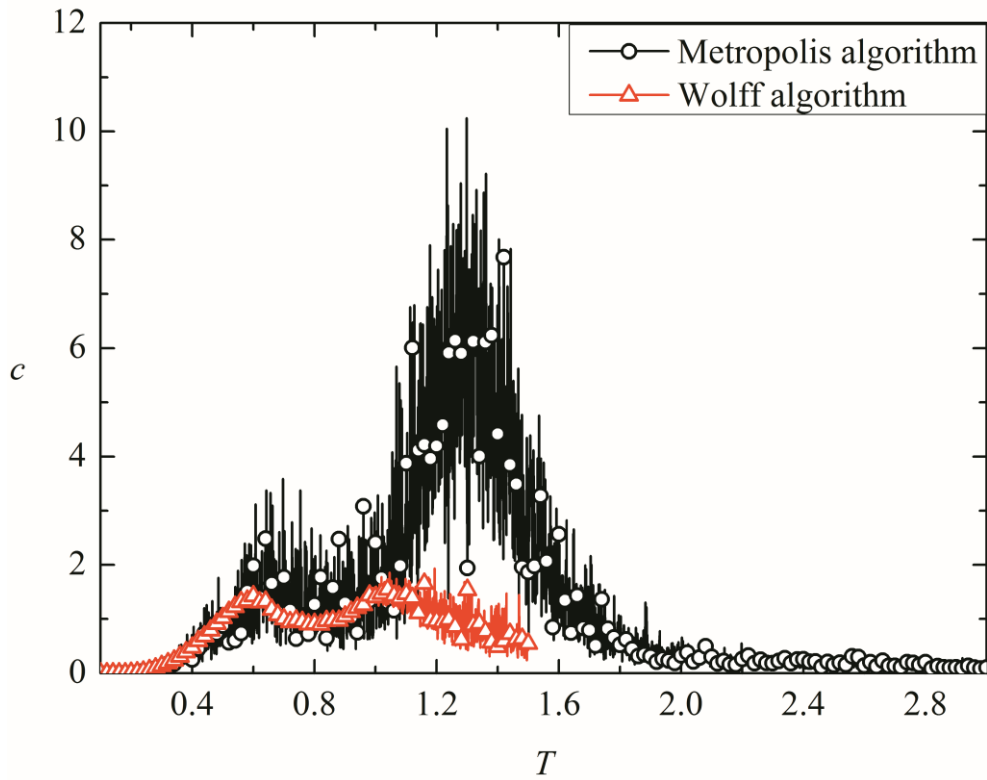


Figure 4.5 The specific heat against temperature for the six-state clock model with lattice size $N=128 \times 128$ obtained by the Metropolis algorithm and the Wolff algorithm.

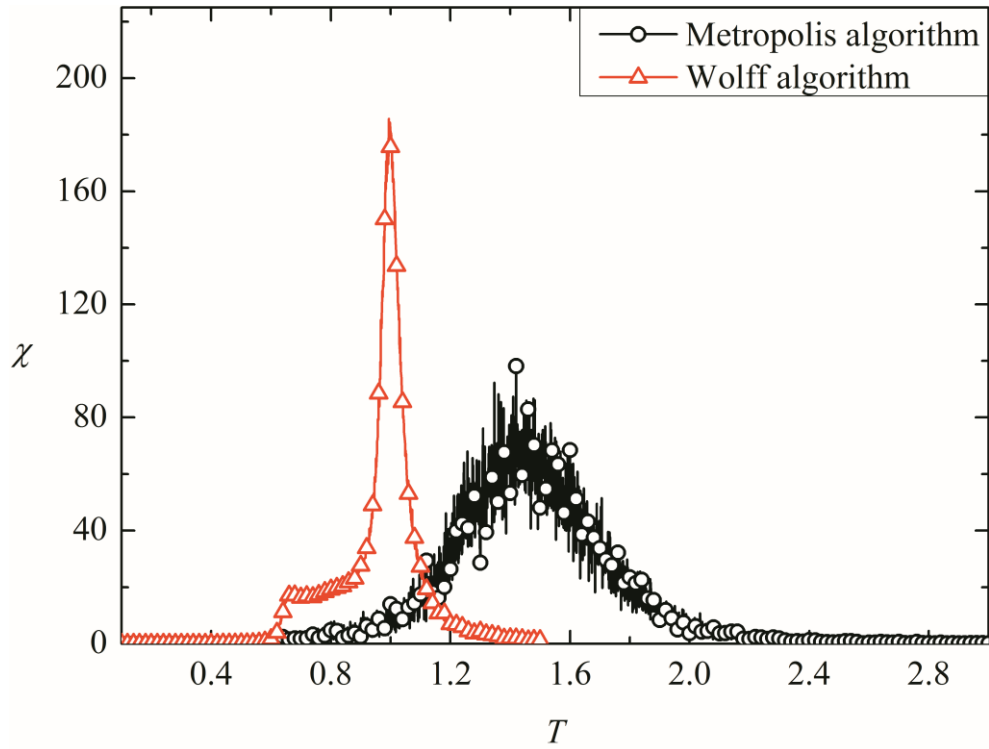


Figure 4.6 The susceptibility against temperature for the six-state clock model with lattice size $N=128\times 128$ obtained by the Metropolis algorithm and the Wolff algorithm.

4.2 Second-order phase transition and KT transition

The four-state clock model ($q=4$) is known to be equivalent to the Ising model ($q=2$). The nature of phase transitions for both cases is essentially the same, being of the second-order type. On the other hand, the phase transition in the six-state clock model ($q=6$) is known to be of the KT-type. Several properties of the clock model with $q=4$ and $q=6$ are calculated under the same conditions to demonstrate the differences between the second-order phase transition and the KT transition in these models.

The magnetization against temperature for the four-state and the six-state clock model with various lattice sizes are given in Figures 4.7 and 4.8, respectively. In four-state clock model, the magnetization is non-zero below the critical temperature and above which it vanishes. The low-temperature ordered phase and the high-temperature disordered phase are separated at the critical temperature, manifesting the second-order phase transition. However, in the six-state clock model, the magnetization undergoes two transitions instead of a single one. There exists an intermediate phase called the KT phase (or the massless phase) between the low-temperature ordered phase and the high-temperature disordered phase.

The specific heat against temperature for the four-state and the six-state clock model with various lattice sizes are given in Figures 4.9 and 4.10, respectively. Also, the susceptibility against temperature for the four-state and the six-state clock model with various lattice sizes are given in Figures

4.11 and 4.12, respectively. In four-state clock model, a single peak emerges in both specific heat and susceptibility. They diverge at the critical temperature as expected in the second-order phase transition. On the other hand, double peaks are observed in the six-state clock model. Again, this is a manifestation of the KT transition. It is found that, in both cases, as the size of the lattice increases, the peaks of both specific heat and susceptibility become sharper. In the four-state clock model, the critical temperature decreases as the lattice size increases. In the six-state clock model, the upper critical temperature also decreases as the lattice size increases, but there is no appreciable effect on the lower critical temperature.

The helicity modulus against temperature for the four-state and the six-state clock model with various lattice sizes are given in Figures 4.13 and 4.14, respectively. In four-state clock model, the helicity modulus remains positive and finite across the transition despite the finite-size effect. However, in the six-state clock model, it vanishes above the critical temperature. In order to demonstrate an abrupt jump in the helicity modulus in six-state clock model, the fourth-order helicity moduli against temperature with various lattice sizes is given in Figure 4.15. It is demonstrated that the fourth-order helicity modulus is negative at the phase transition and thus the discontinuous nature of the helicity modulus is confirmed. Hence the phase transition for the six-state clock model is of the KT-type.

The critical exponent η against temperature for the six-state clock model with various lattice sizes is given in Figure 4.16. The critical

temperature that determined from the critical exponent η and from the helicity modulus are the same. The results are given in Table III. For the largest lattice size $N=128\times 128$, the critical temperature is $T_c=0.916$, which is consistent with the literatures [14-18, 20].

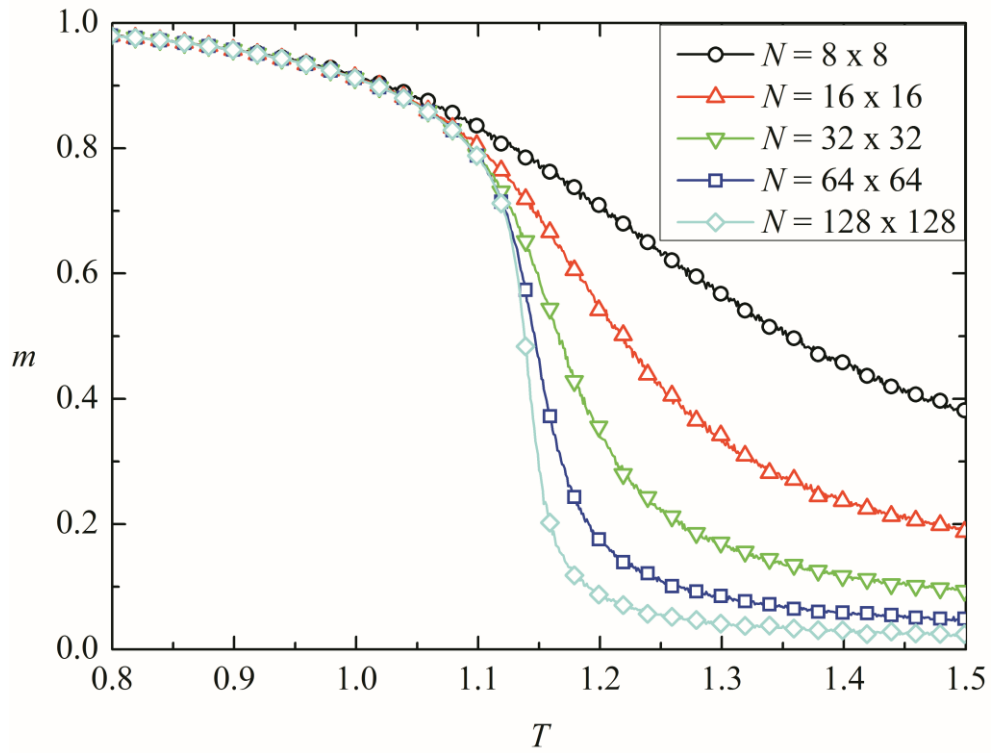


Figure 4.7 The magnetization against temperature for the four-state clock model with various lattice sizes.

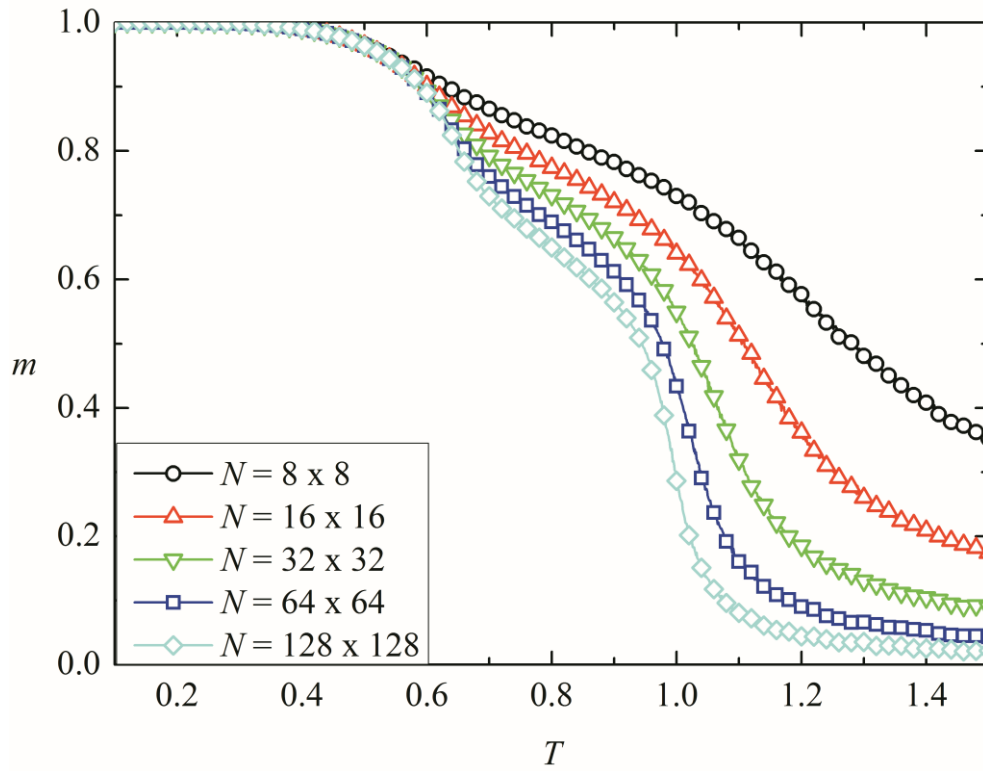


Figure 4.8 The magnetization against temperature for the six-state clock model with various lattice sizes.

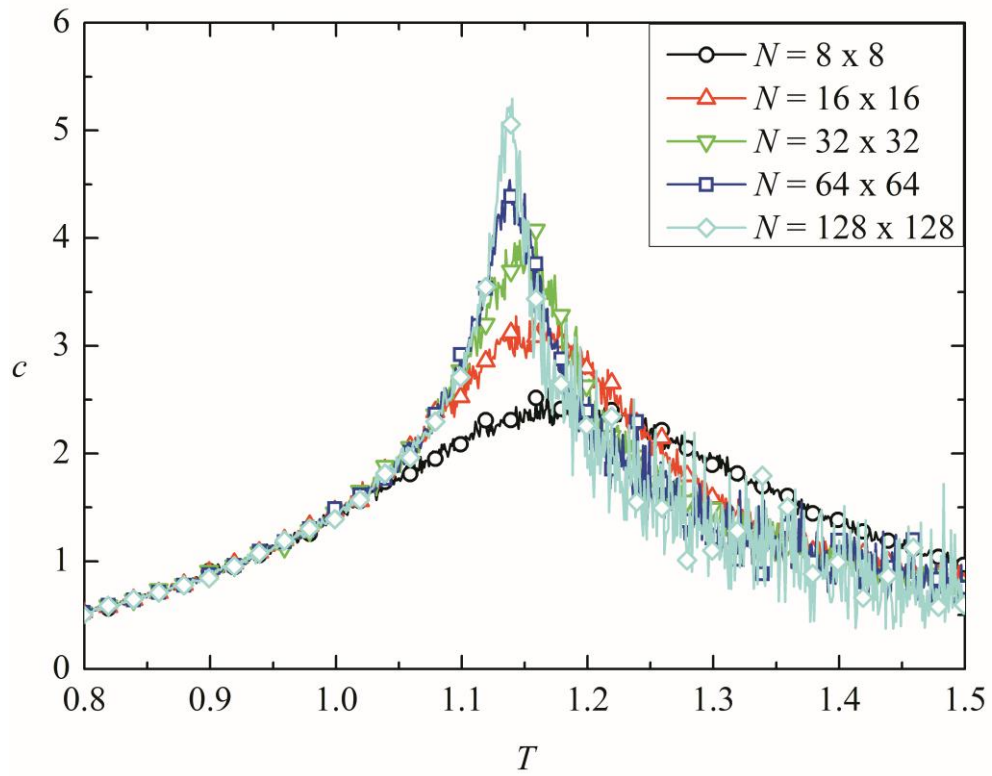


Figure 4.9 The specific heat against temperature for the four-state clock model with various lattice sizes.

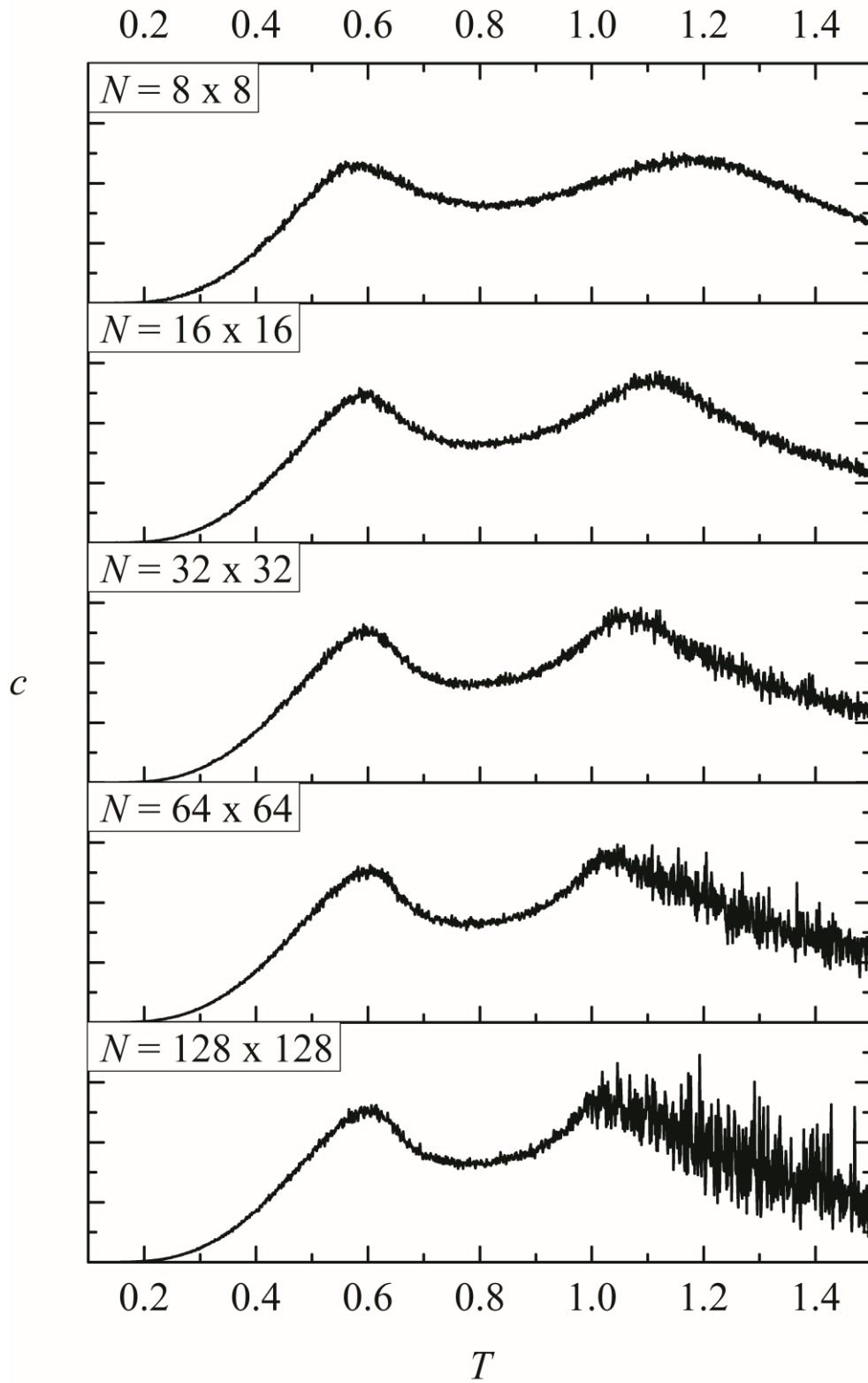


Figure 4.10 The specific heat against temperature for the six-state clock model with various lattice sizes.

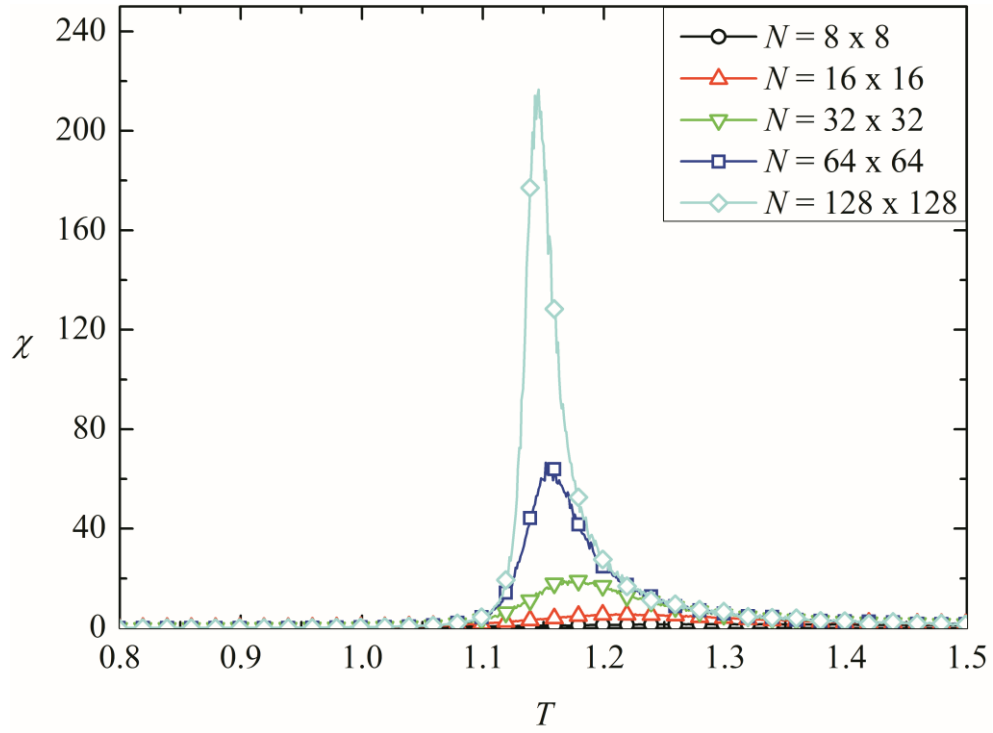


Figure 4.11 The susceptibility against temperature for the four-state clock model with various lattice sizes.

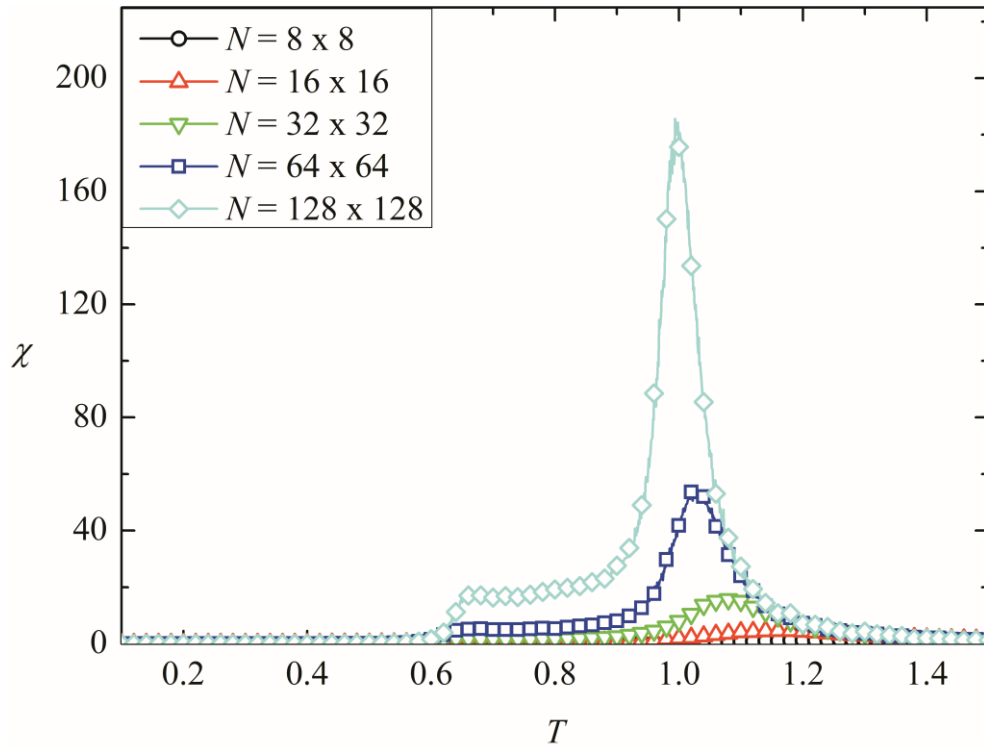


Figure 4.12 The susceptibility against temperature for the six-state clock model with various lattice sizes.

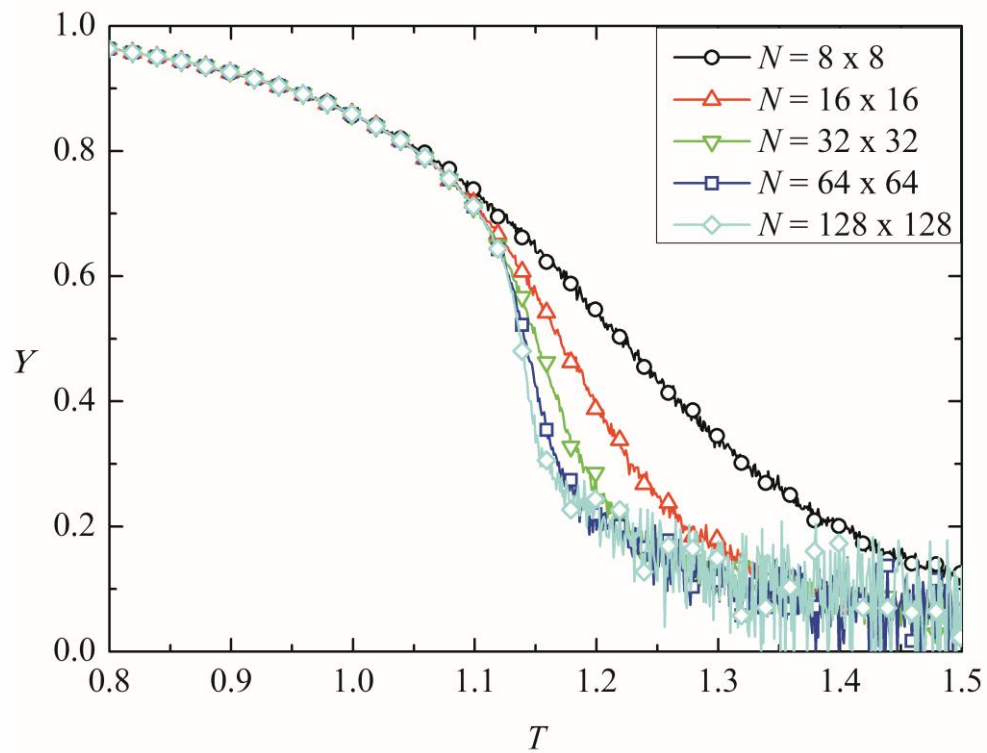


Figure 4.13 The helicity modulus against temperature for the four-state clock model with various lattice sizes.

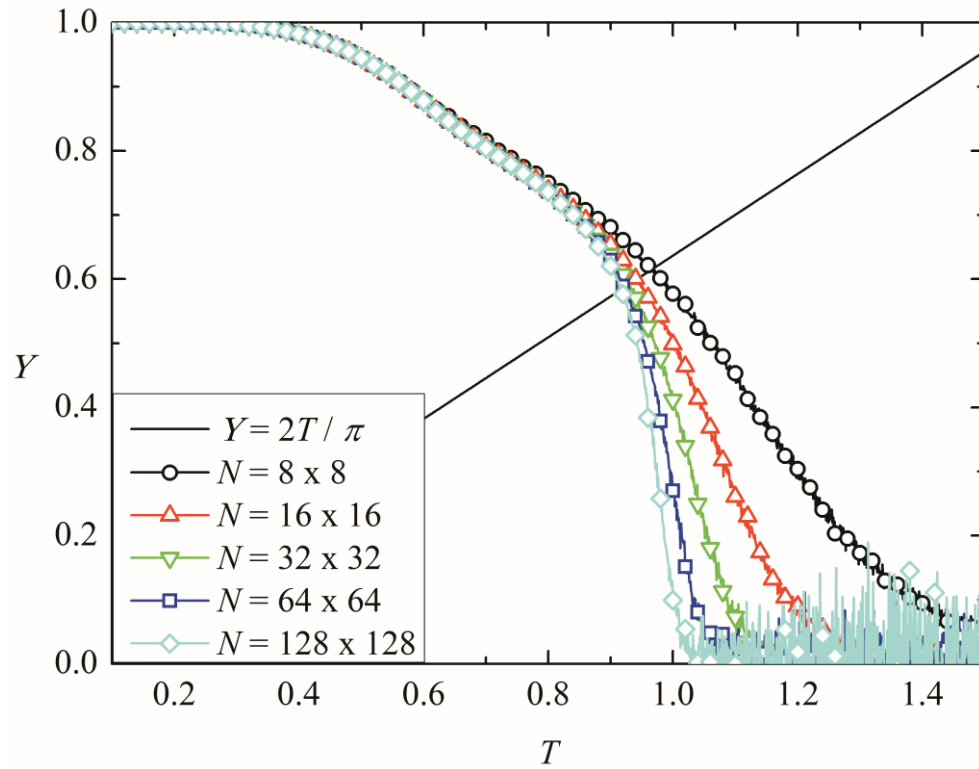


Figure 4.14 The helicity modulus against temperature for the six-state clock model with various lattice sizes.

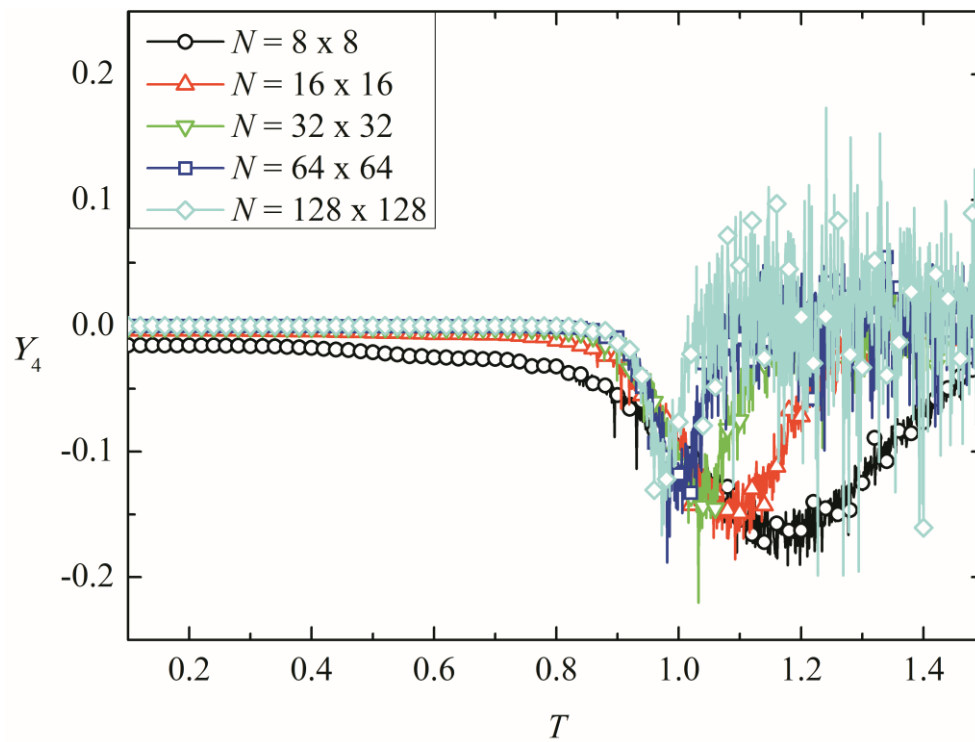


Figure 4.15 The fourth-order helicity modulus against temperature for the six-state clock model with various lattice sizes.

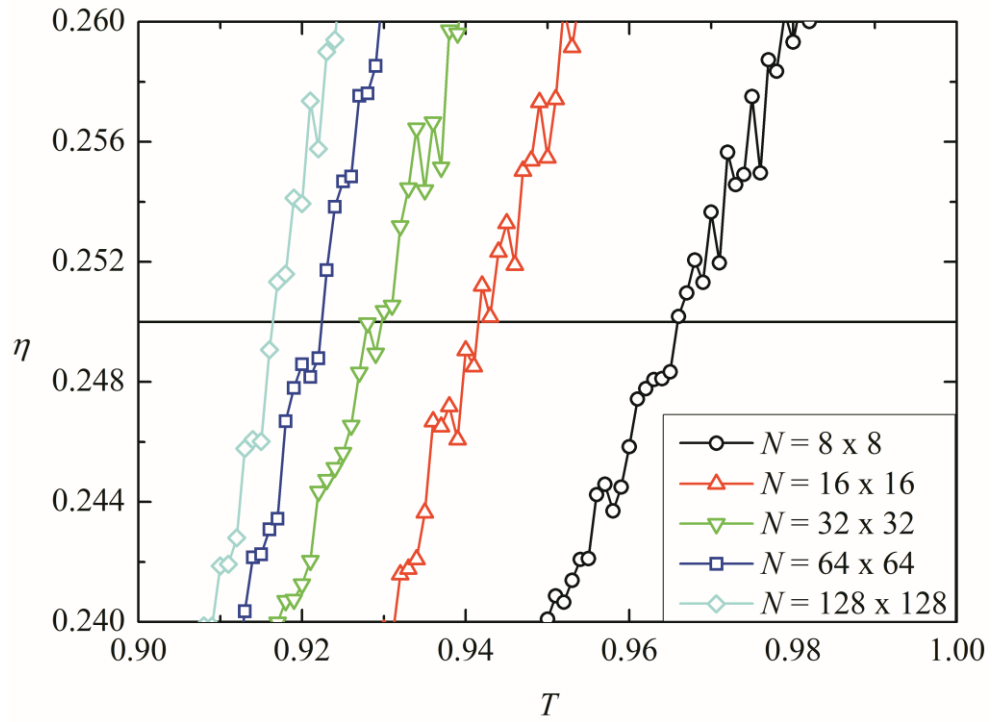


Figure 4.16 The critical exponent η against temperature for the six-state clock model with various lattice sizes.

N	T_c
8×8	0.996
16×16	0.942
32×32	0.930
64×64	0.922
128×128	0.916

Table III The critical temperature for the six-state clock model with various lattice sizes.

4.3 Six-state clock model and eight-state clock model

Since the critical behavior for the q -state clock model does not change appreciably on varying q values when q is large. At the limiting case $q \rightarrow \infty$, where the spin state varies continuously, it restores to the XY model. The results for the eight-state clock model ($q=8$) are shown to demonstrate the phase transition of the q -state clock model for $q \geq 6$ is still of the KT-type as expected.

The magnetization against temperature for the eight-state clock model with various lattice sizes is given in Figure 4.17. In the eight-state clock model, the magnetization also undergoes two transitions instead of a single one. There also exists an intermediate phase between the low-temperature ordered phase and the high-temperature disordered phase. The lower critical temperature of the eight-state clock model is lower than that of the six-state clock model while the upper critical temperature remains approximately the same as that in the six-state clock model. Hence, the intermediate phase in the eight-state clock model is wider than that in the six-state clock model.

The specific heat and the susceptibility for the eight-state clock model with various lattice sizes are given in Figures 4.18 and 4.19, respectively. In the eight-state clock model, double peaks are also observed in both the specific heat and the susceptibility. The height of the peaks in the eight-state clock model is approximately the same as that in the six-state clock model. Again, the results showed that the lower critical temperature in the eight-state clock model is lower than that in the six-state clock model. Also,

the intermediate phase in the eight-state clock model is wider than that in the six-state clock model.

The helicity modulus against temperature for the eight-state clock models with various lattice sizes is given in Figure 4.20. The helicity modulus vanishes above the critical temperature. Furthermore, the fourth-order helicity modulus against temperature for the eight-state clock models with various lattice sizes is given in Figure 4.21. The fourth-order helicity modulus is negative at the phase transition and thus the discontinuous nature of the helicity modulus is confirmed. Hence the phase transition for the eight-state clock model is also of the KT-type as expected.

The results showed that both the six-state and the eight-state clock model undergo KT transition and their critical behaviors are essentially the same. The only difference is that the lower critical temperature in the eight-state clock model is lower than that in the six-state clock model. Hence the intermediate phase in the eight-state clock model is wider than that in the six-state clock model. The results enable us to estimate the critical behavior of the q -state clock model with $q \gg 6$ and even the XY model. These systems should also undergo the KT transition. The upper critical temperature will remain approximately the same with those in the six-state and the eight-state clock model. However, the lower critical temperature will continuously decrease as q increases, until reaching the value of the XY model. Hence, the intermediate phase will become wider as q increases.

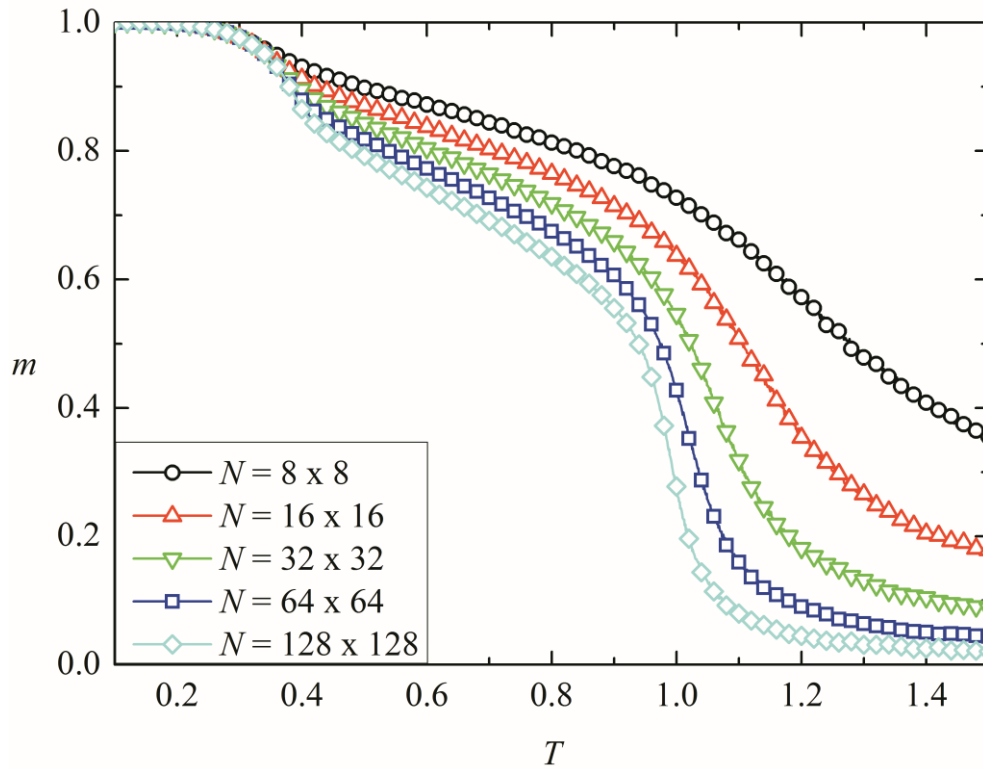


Figure 4.17 The magnetization against temperature for the eight-state clock model with various lattice sizes.

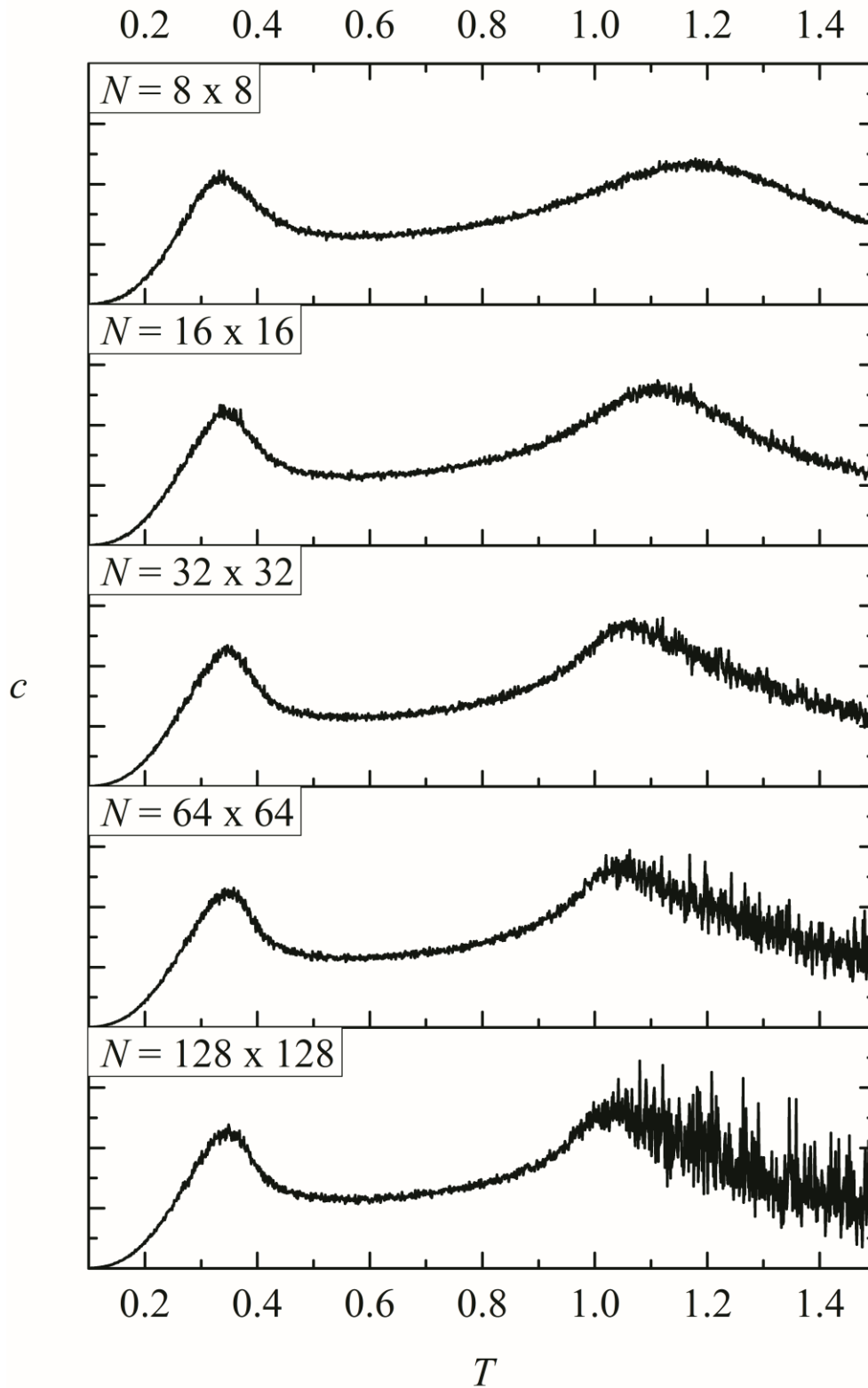


Figure 4.18 The specific heat against temperature for the eight-state clock model with various lattice sizes.

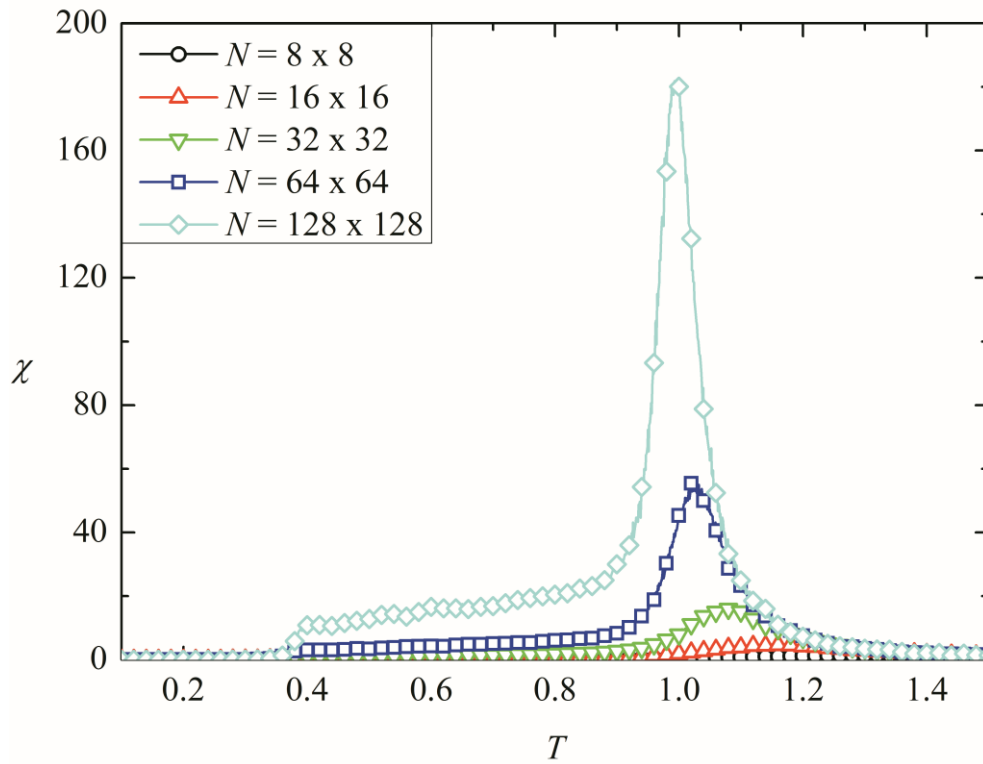


Figure 4.19 The susceptibility against temperature for the eight-state clock model with various lattice sizes.

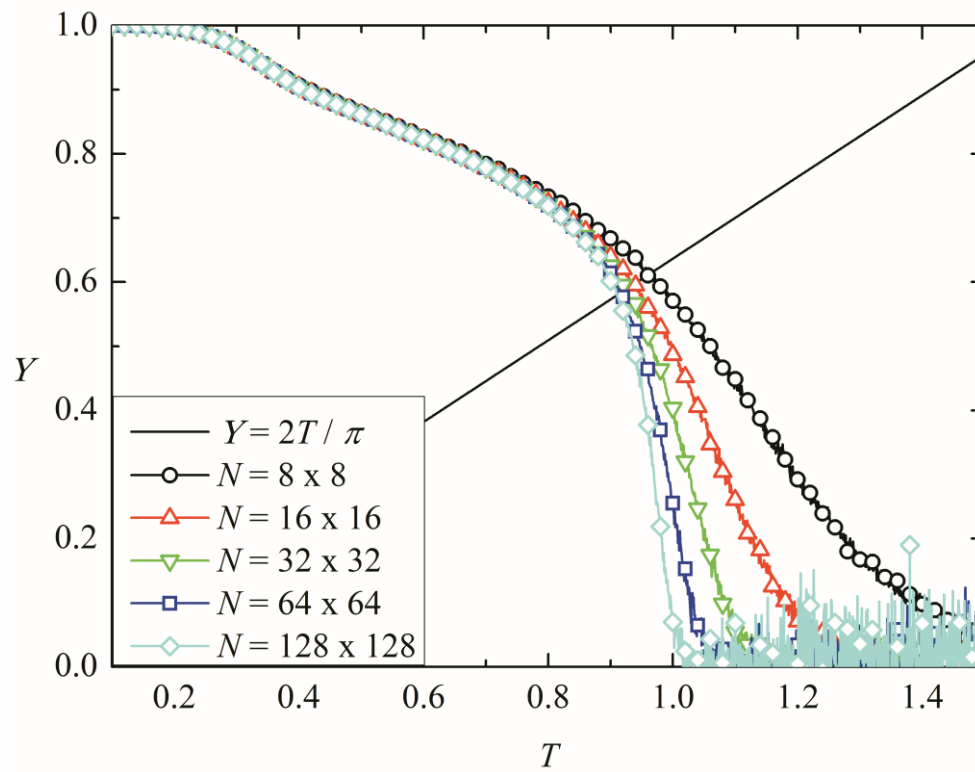


Figure 4.20 The helicity modulus against temperature for the eight-state clock model with various lattice sizes.

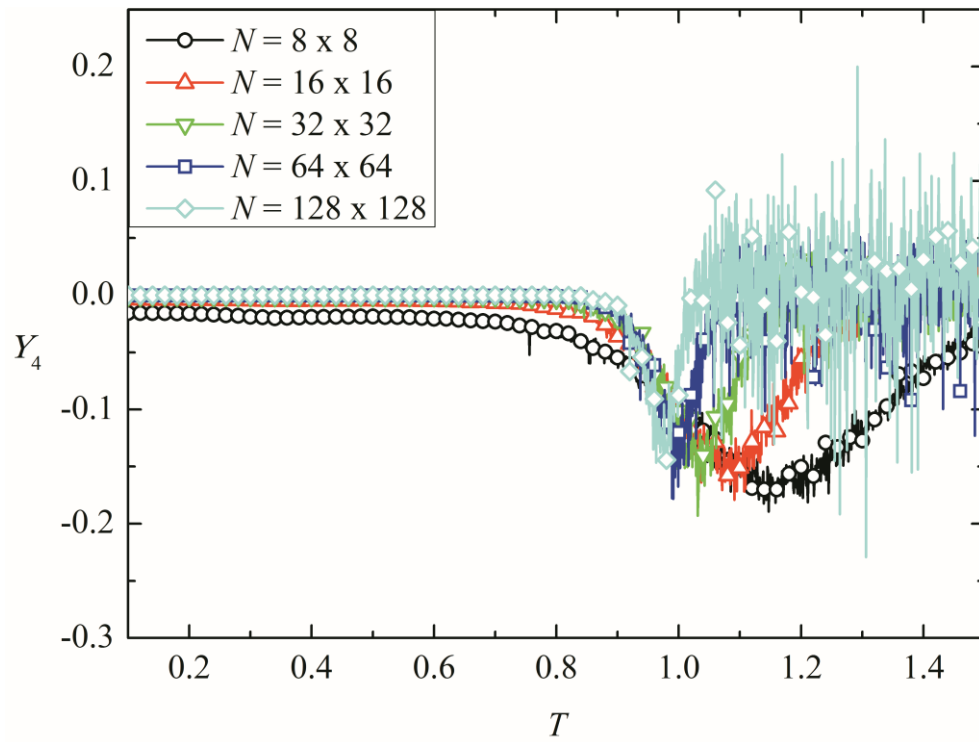


Figure 4.21 The fourth-order helicity modulus against temperature for the eight-state clock model with various lattice sizes.

4.4 Random-bond six-state clock model and random-bond eight-state clock model

From the above results, the KT transition in the pure six-state clock model has been demonstrated. Subsequently, the effects of disorder on the phase transition in the six-state clock model are then investigated. The bond randomness is reflected by the parameter σ as defined in Equation (2.5). The results with lattice size $N = 128 \times 128$ and with different values of σ are shown as follows.

The magnetization against temperature for the random-bond six-state clock model with various σ^2 is given in Figure 4.22. As σ increases, the critical temperature of the system decreases. In the pure system, there exists an intermediate phase between the low-temperature ordered phase and the high-temperature disordered phase. However, as σ increases, this intermediate phase reduces and for $\sigma^2 = 3.0$, it becomes unobservable. In this case, the critical behavior of the magnetization looks very similar to that of the four-state clock model.

The specific heat and the susceptibility against temperature for the random-bond six-state clock model with various σ^2 are given in Figures 4.23 and 4.24, respectively. The results for the specific heat are very noisy especially for large σ . However, we can still be able to identify the double-peak feature as in the pure system for small σ . The results for the susceptibility are much clearer and again the double-peak feature emerges. As σ increases, all the peaks of both specific heat and susceptibility shift

to the left, indicating the decreases in the critical temperature. The distance between the two peaks in the susceptibility decreases as σ increases and for $\sigma^2 = 3.0$, they merge together as one. Furthermore, the height of the peak increases as σ increases and for $\sigma^2 = 3.0$, it becomes comparable to that of the four-state clock model.

The above results for the random-bond six-state clock model showed the shrinkage of the intermediate phase as the amount of disorder (σ) increases. Under a large amount of disorder, the phase transition seems to be of the second-order type as in the four-state clock model. The intermediate phase disappeared and only the low-temperature ordered phase and the high-temperature disordered phase are observed. In order to demonstrate the disappearance of the KT transition under a large amount of disorder, the helicity modulus and the fourth-order helicity modulus of the system are calculated. The helicity modulus against temperature for the random-bond six-state clock model with various σ^2 is given in Figure 4.45. As σ increases, the transition becomes boarder. The helicity modulus still vanishes above the critical temperature for large σ . However, it tends to be continuous rather than makes a discontinuous jump at the transition. The fourth-order helicity modulus against temperature for the random-bond six-state clock model with various σ^2 is given in Figure 4.26. For $\sigma^2 = 0.1$ and $\sigma^2 = 0.5$, the fourth-order helicity modulus at the transition are clearly negative, implying the system undergoes the KT transition. However, despite the noisy nature, the depth of the trough reduces as σ increases. For $\sigma^2 = 3.0$, the trough is no longer observable and thus the helicity modulus does not jump discontinuously. Hence we can conclude

that the transition is no longer of the KT-type and this is consistent with our observations discussed before.

The critical exponent η against temperature for the random-bond six-state clock model with various σ is given in Figure 4.27. Again, the critical temperature that determined from the critical exponent η and from the helicity modulus are the same. The results are given in Table IV. Also, the critical temperature against σ^2 for the random-bond six-state clock model is given in Figure 4.28. Since the transition is no longer of the KT-type for large σ , the critical temperature determined from these methods may be beyond the definitions described above. Hence the results for $\sigma^2 = 2.0$ and $\sigma^2 = 3.0$ are only for comparison purpose.

The driving force behind the KT transition involves the binding and unbinding of the vortex-antivortex pairs. Since these processes are not affected by a small perturbation on the local spin phase angle, under a small amount of disorder, the phase transition is still of the KT-type. However, the binding and unbinding of the vortex-antivortex pairs is prohibited under a large amount of disorder and thus the transition is only determined by the competition between the spin-spin interactions and the thermal fluctuations acting on the system. Hence the transition is no longer of the KT-type and becomes the ordinary first-order or the second-order phase transition. If the amount of disorder is too large, there will be no phase transition in the system, because the ordering of spins cannot be developed.

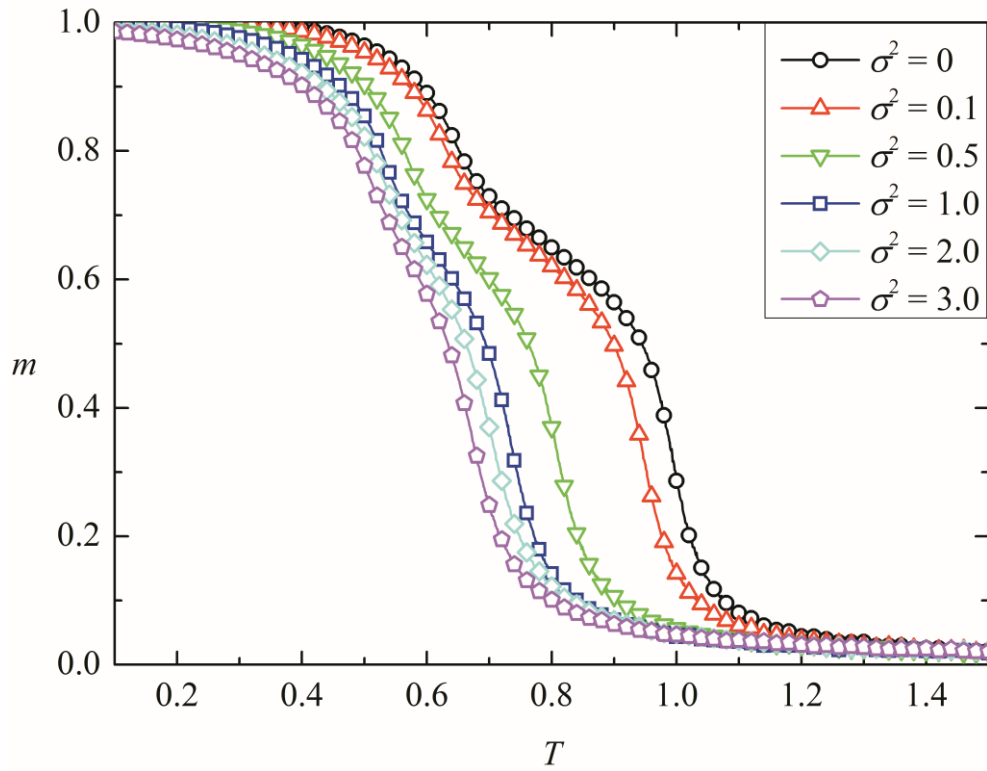


Figure 4.22 The magnetization against temperature for the random-bond six-state clock model with lattice size $N=128\times 128$ and various σ^2 .

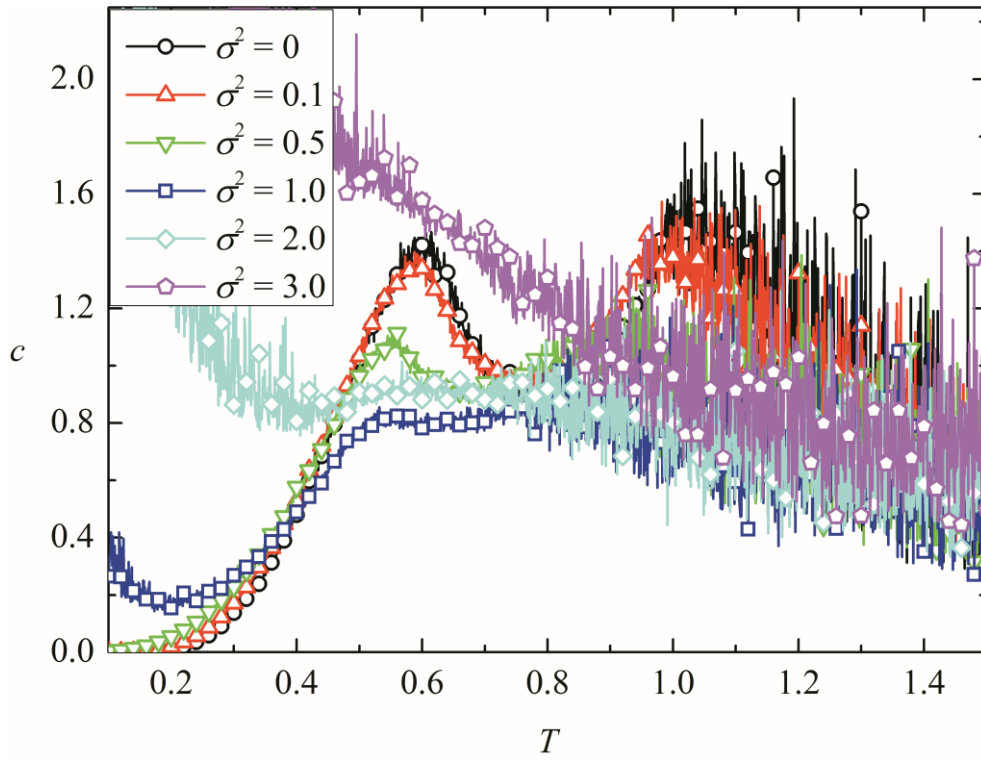


Figure 4.23 The specific heat against temperature for the random-bond six-state clock model with lattice size $N = 128 \times 128$ and various σ^2 .

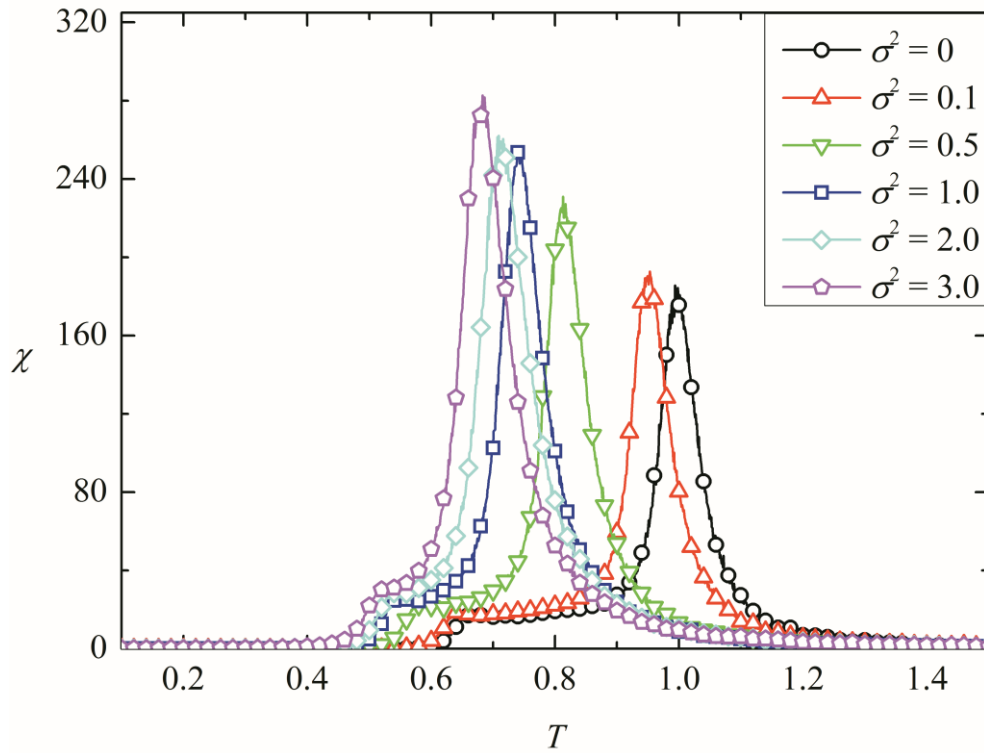


Figure 4.24 The susceptibility against temperature for the random-bond six-state clock model with lattice size $N=128 \times 128$ and various σ^2 .

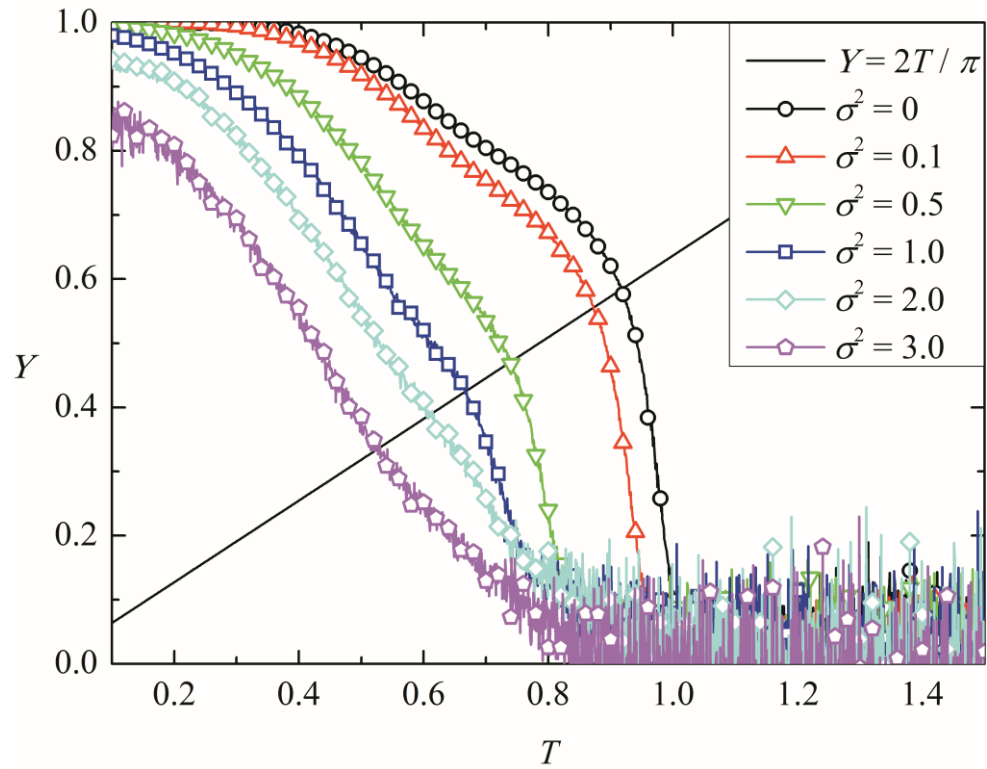


Figure 4.25 The helicity modulus against temperature for the random-bond six-state clock model with lattice size $N=128\times 128$ and various σ^2 .

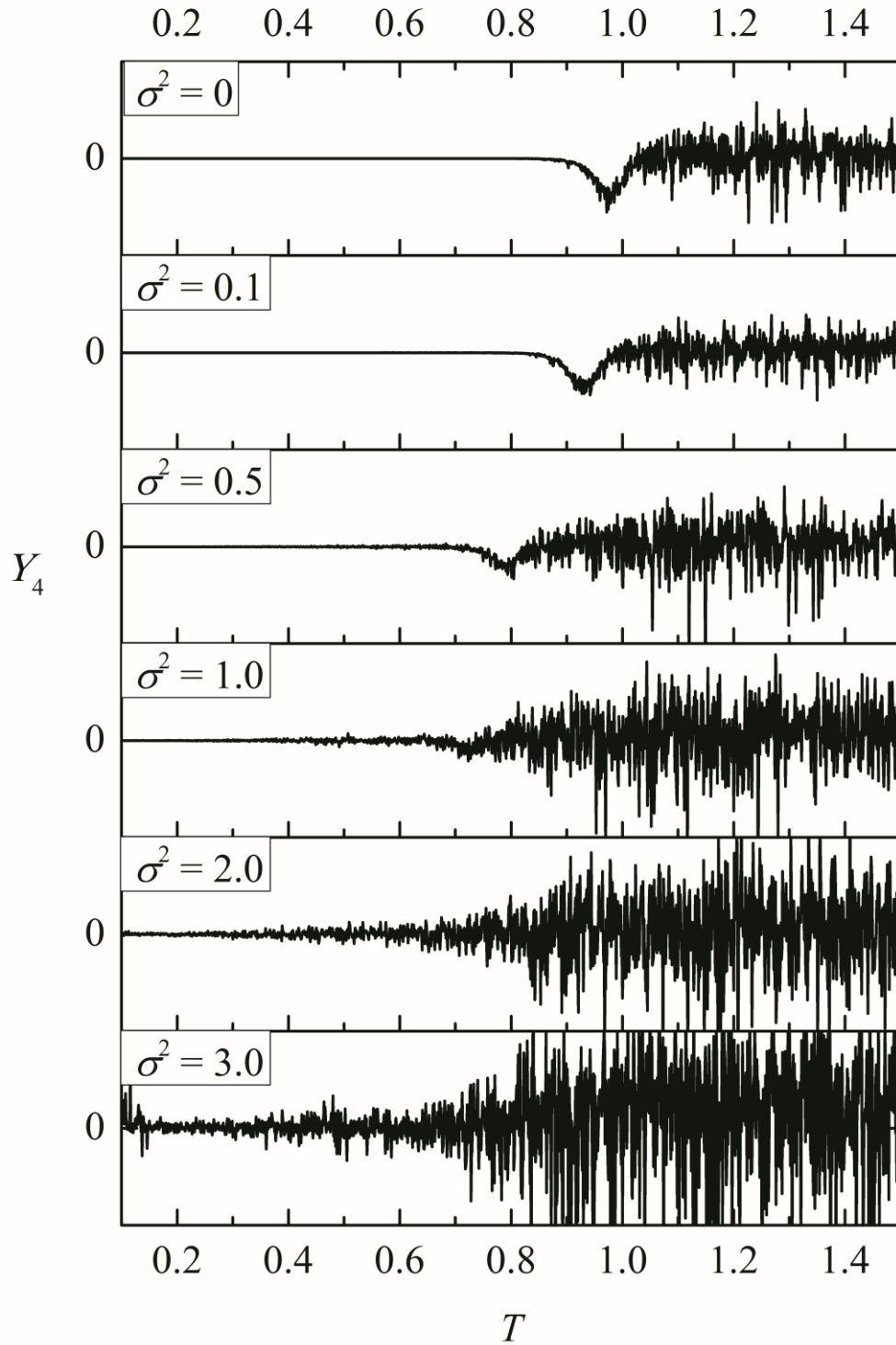


Figure 4.26 The fourth-order helicity modulus against temperature for the random-bond six-state clock model with lattice size $N = 128 \times 128$ and various σ^2 .

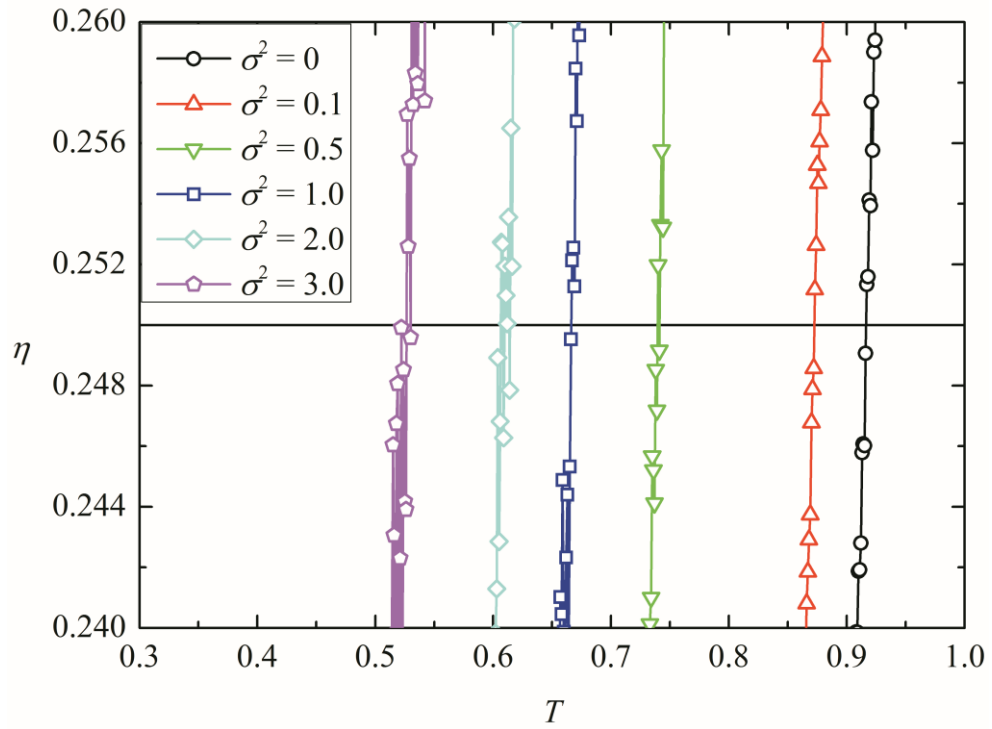


Figure 4.27 The critical exponent η against temperature for the random-bond six-state clock model with lattice size $N = 128 \times 128$ and various σ^2 .

σ^2	T_c
0	0.916
0.1	0.873
0.5	0.741
1.0	0.666
2.0	0.611
3.0	0.526

Table IV The critical temperature for the random-bond six-state clock model with lattice size $N = 128 \times 128$ and various σ^2 .

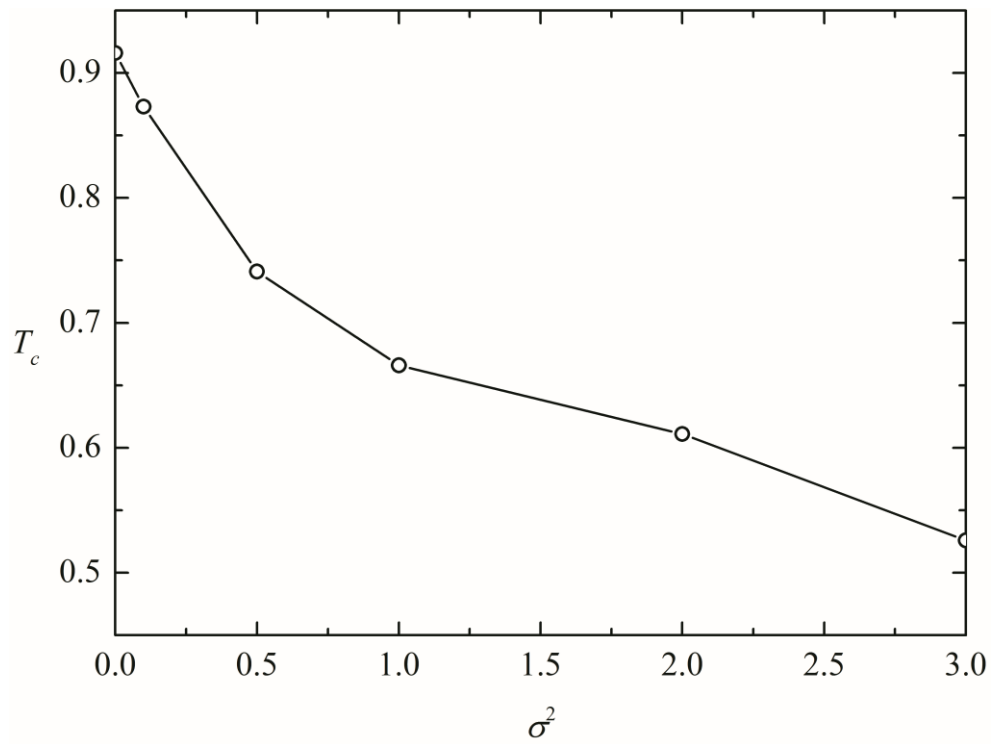


Figure 4.28 The critical temperature against σ^2 for the random-bond six-state clock model with lattice size $N = 128 \times 128$.

Chapter 5 Conclusion

The critical behavior of the clock model in two-dimensional square lattice is studied numerically using Monte Carlo method with Wolff algorithm. It is shown that, the phase transition in the four-state clock model is the same as that in the Ising model, being of the second-order type. On the other hand, the phase transition in the six-state clock model is the same as that in the XY model, being of the KT-type. It is demonstrated that there exists an intermediate phase between the low-temperature ordered phase and the high-temperature disordered phase in the six-state clock model. The results for the four-state clock model and the six-state clock model are compared to show the difference between the second-order phase transition and the KT transition. Since the key characteristic of the KT transition, which is the abrupt jump in the helicity modulus at the transition, is difficult to determine directly by numerical calculations due to limited precision. A new numerical method based on a stability argument is used to verify the discontinuity of the helicity modulus of the system, such that the KT transition is identified. Furthermore, the critical temperature for the six-state clock model is determined from the critical exponent $\eta(T_c) = 1/4$. For the largest lattice size $N = 128 \times 128$, the critical temperature is $T_c = 0.916$, which is consistent with the literatures.

Since the critical behavior for the q -state clock model does not change appreciably on varying q values when q is large. At the limiting case $q \rightarrow \infty$, where the spin state varies continuously, it restores to the XY

model. The critical behavior for the eight-state clock model ($q=8$) is studied to demonstrate the phase transition of the q -state clock model for $q \geq 6$ is still of the KT-type. The results showed that the phase transition in the eight-state clock model is of the KT-type as expected.

To investigate the effects of disorder, the bond randomness is introduced to the system by assuming a Gaussian distribution for the coupling coefficients with the mean $\mu=1$ and different values of variance, from $\sigma^2=0.1$ to $\sigma^2=3.0$. The critical behavior of the random-bond six-state clock model is studied and the critical temperature of the system is determined. The results showed that, a small amount of disorder (small σ) reduces the critical temperature of the system, without altering the nature of transition. However, a larger amount of disorder changes the transition from the KT-type into that of non-KT-type.

Since the driving force behind the KT transition involves the binding and unbinding of the vortex-antivortex pairs. These processes are not affected by a small perturbation on the local spin phase angle, under a small amount of disorder, the phase transition is still of the KT-type. However, the binding and unbinding of the vortex-antivortex pairs is prohibited under a large amount of disorder and thus the transition is only determined by the competition between the spin-spin interactions and the thermal fluctuations acting on the system. Hence the transition is no longer of the KT-type and becomes the ordinary first-order or second-order phase transition. If the amount of disorder is too large, there will be no phase transition in the system, because the ordering of spins cannot be developed.

The effects of disorder on phase transition have attracted many interests. A number of numerical works had studied the effects of non-magnetic impurities on the KT transition. Since non-magnetic impurities can be viewed as lattice vacancies, the results found that the KT transition disappears as the vacancy density reaches the lattice percolation limit. In the real systems, the source of defects may not be only from the non-magnetic impurities but also from the magnetic ones. Our results showed that when the amount of magnetic impurities is large, the KT transition becomes the ordinary first-order or the second-order phase transition, instead of being disappeared.

There are theoretical works conjectured that strong disorder will induce a first-order phase transition in the XY model. In the present work, we cannot conclude whether the phase transition of the random-bond six-state clock model changes to the first-order type or the second-order type. Further investigation is necessary.

References

- [1] J. C. Maxwell, A treatise on Electricity and Magnetism, Vol. I, Oxford University Press, 1873.
- [2] J. C. Maxwell, A treatise on Electricity and Magnetism, Vol. II, Oxford University Press, 1873.
- [3] Einstein, H. A. Lorentz, H. Weyl, and H. Minkowski, The Principle of Relativity, Dover Publications, 1952.
- [4] P. A. M. Dirac, The Principles of Quantum Mechanics, Oxford University Press, 1981.
- [5] L. Onsager, "Crystal Statistics. I. A Two-Dimensional Model with an Order-Disorder Transition," *Physical Review*, vol. 65, no. 3 & 4, p. 117, 1944.
- [6] B. Kaufman and L. Onsager, "Crystal Statistics. III. Short-Range Order in a Binary Ising Lattice," *Physical Review*, vol. 76, no. 8, p. 1244, 1949.
- [7] F. Y. Wu, "The Potts model," *Reviews of Modern Physics*, vol. 54, no. 1, p. 235, 1982.
- [8] L. D. Landau and E. M. Lifshitz, Statistical Physics, Part 1, Butterworth-Heinemann, 1980.
- [9] E. M. Lifshitz and L. P. Pitaevskii, Statistical Physics, Part 2, Butterworth-Heinemann, 1980.
- [10] J. M. Kosterlitz and D. J. Thouless, "Ordering, metastability and phase

- transitions in two-dimensional systems," *J. Phys. C: Solid State Phys.*, vol. 6, p. 1181, 1973.
- [11] J. M. Kosterlitz, "The critical properties of the two-dimensional xy model," *J. Phys. C: Solid State Phys.*, vol. 7, p. 1046, 1974.
- [12] David R. Nelson and J. M. Kosterlitz, "Universal Jump in the Superfluid Density of Two-Dimensional Superfluids," *Physical Review Letters*, vol. 39, no. 19, p. 1201, 1977.
- [13] J. Ashkin and E. Teller, "Statistics of Two-Dimensional Lattices with Four Components," *Physical Review*, vol. 64, no. 5 & 6, p. 178, 1943.
- [14] Seiji Miyashita, Hidetoshi Nishimori, Akira Kuroda, and Masuo Suzuki, "Monte Carlo Simulation and Static and Dynamic Critical Behavior of the Plane Rotator Model," *Progress of Theoretical Physics*, vol. 60, no. 6, p. 1669, 1978.
- [15] J. Tobochnik, "Properties of the q-state clock model for q=4, 5, and 6," *Physical Review B*, vol. 26, no. 11, p. 6201, 1982.
- [16] M. S. S. Challa and D. P. Landau, "Critical behavior of the six-state clock model in two dimensions," *Physical Review B*, vol. 33, no. 1, p. 437, 1986.
- [17] Atsushi Yamagata and Ikuo Ono, "Phase transitions of the 6-clock model in two dimensions," *J. Phys. A: Math. Gen.*, vol. 24, p. 265, 1991.
- [18] Yusuke Tomita and Yutaka Okabe, "Probability-changing cluster algorithm for two-dimensional XY and clock models," *Physical Review B*, vol. 65, p. 184405, 2002.

- [19] C.-O. Hwang, "Six-state clock model on the square lattice: Fisher zero approach with Wang-Landau sampling," *Physical Review E*, vol. 80, p. 042103, 2009.
- [20] S. K. Baek, P. Minnhagen, and B. J. Kim, "Comment on "Six-state clock model on the square lattice: Fisher zero approach with Wang-Landau sampling," *Physical Review E*, vol. 81, p. 063101, 2010.
- [21] Seung Ki Baek and Petter Minnhagen, "Non-Kosterlitz-Thouless transitions for the q-state clock models," *Physical Review E*, vol. 82, p. 031102, 2010.
- [22] Eytan Domany, David Mukamel, and Adam Schwimmer, "Phase diagram of the $Z(5)$ model on a square lattice," *J. Phys. A: Math. Gen.*, vol. 13, p. L311, 1980.
- [23] O. Borisenko, G. Cortese, R. Fiore, M. Gravina, and A. Papa, "Numerical study of the phase transitions in the two-dimensional $Z(5)$ vector model," *Physical Review E*, vol. 83, p. 041120, 2011.
- [24] A. B. Harris, "Effect of random defects on the critical behavior of Ising models," *J. Phys. C: Solid State Phys.*, vol. 7, p. 1671, 1974.
- [25] S. Chen, Alan M. Ferrenberg, and D. P. Landau, "Randomness-Induced Second-Order Transition in the Two-Dimensional Eight-State Potts Model: A Monte Carlo Study," *Physical Review Letters*, vol. 69, no. 8, p. 1213, 1992.
- [26] J. J. Alonso, "Phase transitions in systems of magnetic dipoles on a square lattice with quenched disorder," *Journal of Magnetism and Magnetic Materials*, vol. 322, p. 1330, 2010.

- [27] S. A. Leonel, Pablo Zimmermann Coura, A. R. Pereira, L. A. S. Mol, and B. V. Costa, "Monte Carlo study of the critical temperature for the planar rotator model with nonmagnetic impurities," *Physical Review B*, vol. 67, p. 104426, 2003.
- [28] Tasrief Surungan and Yutaka Okabe, "Kosterlitz-Thouless transition in planar spin models with bond dilution," *Physical Review B*, vol. 71, p. 184438, 2005.
- [29] G. M. Wysin, A. R. Pereira, I. A. Marques, S. A. Leonel, and P. Z. Coura, "Extinction of the Berezinskii-Kosterlitz-Thouless phase transition by nonmagnetic disorder in planar symmetry spin models," *Physical Review B*, vol. 72, p. 094418, 2005.
- [30] S. E. Korshunov, "Disorder-induced first order transition in superconducting films," *Physical Review B*, vol. 46, no. 10, p. 6615, 1992.
- [31] P. Minnhagen and B. J. Kim, "Direct evidence of the discontinuous character of the Kosterlitz-Thouless jump," *Physical Review B*, vol. 67, p. 172509, 2003.
- [32] Alan M. Ferrenberg, D. P. Landau, and Y. Joanna Wong, "Monte Carlo Simulations: Hidden Errors from "Good" Random Number Generators," *Physical Review Letters*, vol. 69, no. 23, p. 3382, 1992.
- [33] N. Metropolis, A. W. Rosenbluth, M. N. Rosenbluth, A. H. Teller, and E. Teller, "Equation of State Calculations by Fast Computing Machines," *The Journal of Chemical Physics*, vol. 21, no. 6, p. 1087, 1953.

- [34] U. Wolff, "Collective Monte Carlo Updating for Spin Systems,"
Physical Review Letters, vol. 62, no. 4, p. 361, 1989.
- [35] J. S. Wang and R. H. Swendsen, "Cluster Monte Carlo Algorithms,"
Physica A, vol. 167, p. 565, 1990.